Energy, Mines and Resources Canada
Énergie, Mines et Ressources Canada

CANMET
Canada Centre for Mineral and Energy Technology
Centre canadien de la technologie des minéraux et de l'énergie

THE USE OF CYCLIC VOLTAMMETRY AND SEM/EDX TECHNIQUES TO CHARACTERIZE THE BEHAVIOUR OF COPPER ANODES CONTAINING VARIOUS IMPURITIES DURING ELECTROREFINING

E.A. Kucharska-Giziewicz and D.J. MacKinnon
Resource Utilization Laboratory

July 1992

This document is an unedited interim report prepared primarily for discussion and interactive reporting purposes. It does not represent a final expression of the opinion of the Canada Centre for Mineral and Energy Technology (CANMET)

Ce document est un rapport provisoire non-révisé préparé principalement pour fin de discussion et de documentation interne. Il ne représente nullement l'expression définitive de l'opinion du Centre canadien de la technologie des minéraux et de l'énergie (CANMET)

56 pp

Project: 30.20.01 (0748)
Copper Refining Project

MINERAL SCIENCES LABORATORIES
DIVISION REPORT MSL 92-47 (TR)

MICROMEDIA

Crown Copyrights Reserved

THE USE OF CYCLIC VOLTAMMETRY AND SEM/EDX TECHNIQUES TO CHARACTERIZE THE BEHAVIOUR OF COPPER ANODES CONTAINING VARIOUS IMPURITIES DURING ELECTROREFINING

by

E.A. Kucharska-Giziewicz* and D.J. MacKinnon**

ABSTRACT

A reproducible technique using cyclic voltammetry has been developed to characterize the behaviour of impurity-containing copper anodes during electrorefining. The method involves cycling the anode potential at a rate of 2 mV/s between the open circuit potential of -0.35 V and 0.0V vs the mercury/mercurous sulphate (MSE) reference electrode. The shape of the cyclic voltammogram changes with continuous cycling depending on the type and concentration of the anode impurity. These shape changes also can indicate the tendency of the anode to passivate. A strong correlation between the electrochemical behaviour of the copper anodes and their impurity contents was found. Scanning electron microscopy with an energy dispersive X-ray analysis system was used to examine the corroded surfaces of the anodes.

Keywords: copper, electrorefining, anode passivation, impurity effects, cyclic voltammetry, SEM/EDX.

---

* Research Technologist and ** Research Scientist, Mineral Sciences Laboratories, CANMET, Energy, Mines and Resources Canada, 555 Booth Street, Ottawa, Ontario K1A 0G1.

1

INTRODUCTION

In a previous investigation (1), laboratory conditions were established that resulted in reproducible and predictable electrochemical characteristics for the corrosion of copper anodes. A reproducible technique using cyclic voltammetry (CV) was developed to characterize the behaviour of silver-containing copper anodes during electrorefining. The method involved cycling the anode potential at a rate of 2 mV/s between the open circuit potential of -0.35 V vs MSE and 0.0 V. The shape of the CV changed with continuous cycling depending on the concentration of silver in the copper anode. As a result of continuous cycling, the anodic current decreased dramatically due to the formation of a slimes layer on the anode surface. This slimes layer consisted of a mixture of copper and silver powders, or exclusively of silver powder for high silver anodes. The presence of the slimes layer on the anode surface also resulted in the formation of a second peak during the forward scan of the CV. The ease of formation of this second peak was dependent on the silver content of the anode suggesting that the number of continuous cycles needed to form this peak could be correlated to the ease of anode passivation. It was also established that if the slimes layer is removed by rising and gentle cleaning with a tissue and the potential cycling is then resumed, the formation of the second peak is delayed. This suggests that continuously cycling the potential has "conditioned" the surface such that the anode becomes less susceptible to passivation.

During the previous study (1), selenium- and oxygen-containing anodes were briefly examined. These anodes also produced characteristic changes in the CVs. The present study was undertaken to investigate the selenium- and oxygen-containing anodes in more detail, to confirm the "conditioning" effect of the continuous cycling of the potential on these anodes, to apply the technique to three industrial copper anodes and to examine the "conditioned" surfaces in the SEM. A synthetic anode containing 0.3% Ni + 0.3% O was also examined.

EXPERIMENTAL

Copper rods measuring approximately 20 cm long by 5 cm in diameter and containing various amounts of oxygen, silver, selenium and nickel were prepared for CANMET by the Noranda Technology Centre. Samples of commercial copper anodes were obtained from Noranda's CCR Division, Falconbridge's Kidd Creek Division and Hudson Bay Mining and Smelting Co. (HBMS). A listing of the synthetic and commercial anodes used in this study is presented in Table 1. Typical impurity concentrations of the commercial anodes are presented in Table 2.

Anodes were prepared by cutting rectangular sections from the synthetic and commercial samples. The sections were mounted in acrylic such that only a single face was exposed to the electrolyte. Electrical contact was achieved by drilling through the back of the acrylic mount into the copper specimen. A brass rod was threaded into the copper specimen and this served as the external electrical contact. The brass rod was insulated from the electrolyte by a tight-fitting sleeve of tygon tubing which was sealed into the acrylic mount using silicone rubber. A schematic drawing of the assembled anode is shown in Figure 1.

Cyclic voltammetry studies were performed using a conventional water-jacketed cell with a copper anode as the working electrode, a platinum counter electrode and a mercury/mercurous sulphate reference electrode, Figure 2. A Luggin capillary, the tip of which was set at a distance of about 1 cm from the surface of the working electrode, was used to minimize uncompensated resistance effects caused by an ohmic drop. A PAR 173 potentiostat/galvanostat, equipped with plug-in module M 276, was used as a potentiostat allowing the working electrode of the electrochemical cell to be maintained at various programmed potentials with respect to the reference electrode. A PAR voltage function generator provided various potentiodynamic voltage vs time programs. I-V profiles were recorded using a Hewlett-Packard X-Y recorder.

All of the cyclic voltammetry experiments were conducted in aqueous solutions containing 40 g/L Cu and 160 g/L H_2SO_4 at 65°C as these conditions approximate those used in commercial electrorefining operations. The cell electrolyte was heated and maintained at the desired temperature using a circulating water bath. Experiments were performed in an air atmosphere.

The copper anodes, containing known amounts of impurities, were subjected to a controlled number of continuing cycles ranging between -0.35 V and 0.0 V at a scan speed of 2 mV/s. The anodes were always disconnected at the "cathodic end" of the sweep (at -0.35 V), and usually after 23 or 30 cycles. After removal from the electrochemical cell, each anode was rinsed thoroughly and the excess product layer was removed carefully with a tissue. Each anode was then inserted back into the cell and the experiment was continued in the same fashion. The potential range of -0.35 V to 0.0 V was chosen because of the distinct differences in the electrochemical characteristics displayed by copper electrodes with various impurity contents in this potential region. The scan speed of 2 mV/s was chosen after establishing that the potential at which the peaks form is scan speed dependent.

After the desired experimental conditions were achieved and the experiment was completed, some of the anodes were removed from the cell, immediately rinsed with doubly distilled water, dried and examined in the scanning electron microscope.

RESULTS AND DISCUSSION

A typical cyclic voltammetric profile obtained during continuous potential cycling of a silver-containing copper anode is shown in Figure 3. In the first cycle (1), there is a long gradual slope, which ends in a gradual curve showing some oscillations in the reverse scan. After several cycles (2), the cyclic voltammetric profile shows a firmly rounded peak (First Peak). A small sharp peak is formed followed by very heavy oscillations in the reverse scan. As the cycling continues, the transformation of the curve progresses (3). The curve now ends in a very well defined first peak approximately in the area of the oscillations of the

first cycle. The line then goes upwards to form another well defined peak (Second Peak), before turning around at the beginning of the reverse scan. The oscillations move towards more negative potentials, and when the silver content is $>0.5\%$, they disappear altogether.

Examination of Figure 3 demonstrates that the cyclic voltammogram of a copper electrode containing silver, recorded in the potential range between -0.35 V and 0.0 V, consists of five distinct regions, which are marked A to E on the figure.

(A) - copper dissolution where the current is proportional to the voltage;

(B) - formation of the first peak; i.e., a current maximum resulting from the accumulation of reaction products on the anode surface;

(C) - a second peak starts to develop with time, and as more silver powder accumulates on the electrode surface. At the same time, the first peak shifts towards more negative potentials;

(D) - oscillation; related to the loosening of the surface layer; and

(E) - regular dissolution curve re-established along the same slope as the initial dissolution (A).

As a result of continuous cycling, the anodic current decreases dramatically. The surface of the anode is covered with a mixture of copper and silver powders, or exclusively with silver powder for high silver content electrodes.

Figures 4-18 display the cyclic voltammetric profiles of the electrodes investigated in the course of this research. Each figure shows the average performance of individual electrodes; every measurement was repeated several times to demonstrate the full reproducibility of the electrochemical behaviour. Unless otherwise noted in the figure caption, all the CV profiles show the 1st, 4th and 23rd cycles so that the responses of the various electrodes can be readily compared. These CV profiles exhibit the same characteristics as those described in Figure 3 except that in some cases the second peak does not form, only partially forms or forms and then disappears with continuous cycling of the

potential. In those cases when the second peak does form, its shape appears to depend on the type of impurity present in the copper anode.

The CV profiles for a pure copper anode, Figure 4, indicate that the second peak does not form and that even the oscillations disappear as the number of cycles increases. This behaviour was attributed (1) to the fact that many copper flakes separated from the anode surface every time the cycle passed through the oscillation stage. Figure 5 shows the gradual formation of a strong, well-defined second peak obtained for the anode containing 0.1% Ag. As this peak develops, the oscillations begin to diminish. In the case of Ag, as discussed previously (1), the reaction products remain on the surface during the reverse scan. At 1.0% Ag, the second peak forms much sooner and the oscillations have ceased by the 4th cycle, Figure 6. By cycle 23, the second peak is more established and occurs at less anodic potentials than that for the 0.1% Ag-containing anode; cf., Figures 5 and 6.

Although the second peak begins to form by cycle 6, in the case of the 0.1% Se-containing anode, Figure 7, it has not developed substantially by the 23rd cycle, presumably due to partial flaking of the reaction products. The 1.0% Se-containing anode, however, has a well-developed second peak, Figure 8, again indicating that the concentration of the impurity in the anode is a significant factor. Also, although the second peak for Se is similar to that for Ag during the early stages, by cycle 23, it becomes much broader; cf., Figures 6 and 8.

A series of CV profiles for the 0.1% O-containing anode is presented in Figures 9 and 10. Although the 6th cycle, Figure 9, indicates that the second peak is forming, it has not done so completely by cycle 23. The 23rd cycle, Figure 9, is quite different from those presented so far in that instead of a well-rounded first peak, there is a broadening into a current plateau. Examination of some of the cycles between the 6th and 23rd cycles, Figure 10, reveals that during the 12th cycle, the surface layer has flaked from the anode as indicated by a current maximum in the reverse scan. In cycle 13, the layer again begins to re-establish itself on the surface.

Increasing the oxygen content of the anode to 1.0%, produces a well-formed second peak during the 23rd cycle, Figure 11, as was the case for the 1.0% Ag- and 1.0% Se-containing anodes; however, the shape of this peak was different from the latter two peaks; cf., Figures 1, 6 and 8.

A series of CV profiles obtained for copper anodes containing 0.1% Ag + 0.1% Se is shown in Figures 12 and 13. An interesting feature of this anode is that there was virtually no hysteresis on the initial cycle, Figure 12 (A). By the 4th cycle (Figs. 12-13), there is a well-rounded first peak, oscillations on both the forward and reverse scans and the formation of the second peak is noticeable. By the 23rd cycle, Figure 12 (C), however, the profile is much different than those obtained for anodes individually containing 0.1% Ag, Figure 5 (C) or 0.1% Se, Figure 7 (C), in that there is no longer a second peak on the forward cycle of the scan. As indicated in Figure 13, the second peak continues to grow and the oscillations diminish, cycles 6 and 9, Figure 13 (A), (B), but by cycle 16, Figure 13 (C), the second peak has almost disappeared. Thus, this anode behaves like the 0.1% Se anode rather than the 0.1% Ag anode; in fact, cycle 16, Figure 13 (C), very closely resembles cycle 23, (Figure 7 (C)). The disappearance of the second peak indicates that the surface layer formed during cycling breaks down and falls from the surface.

The effect of continuous potential cycling on a synthetic copper anode containing 0.3% Ni + 0.3% O is shown in Figures 14 and 15. In this case also, the first cycle, Figure 14 (A), shows no hysteresis; cf., Figure 12 (A). Although masked by heavy oscillations on both the forward and reverse scans, the second peak is detectable by cycle 6, Figure 14 (B). However, in cycle 23, Figure 14 (C), the second peak is barely noticeable between the intense oscillations on the forward and reverse scans. However, cycle 23, Figure 14 (C), indicates the reformation of the second peak as revealed by observing the 20th, 21st and 22nd cycles, Figure 15. The 20th cycle, Figure 15 (A), shows a well-developed second peak sandwiched between oscillations on the forward and reverse scans. The second peak is fully developed on the 21st cycle, Figure 15 (B); the forward oscillations have disappeared and the reverse oscillations are diminished. The increase in current

following the oscillations on the reverse scan is associated with the separation of the product layer from the anode surface. Consequently in the next cycle, the 22nd, Figure 15 (C), the oscillations have increased and the second peak begins to reform.

The cyclic voltammograms obtained for the three commercial anodes are shown in Figures 16-18. The first cycles of these scans differ significantly from those obtained for the synthetic anodes, Figures 4-15. For the commercial anodes the first peak is already well-formed, particularly in the case of the Kidd Creek anode, Figure 18 (A). Both the Kidd Creek and CCR anodes, Figures 18 (A) and 17 (A), respectively, have oscillations on both the forward and reverse scans of the first cycle. The first cycle for the HBMS anode, Figure 16 (A), is not as fully-developed as those for the latter two anodes. This difference could be due to the type and concentration of impurities contained in the various anodes. The HBMS anode is the purest of the three anodes, the major impurities being 0.13-0.15% O and $\approx$0.1% Se, Table 2. All the commercial anodes feature a well-formed second peak by the 6th or 7th cycle, that continues to intensify with increasing continuous scans.

By the 23rd cycle, the second peak for the HBMS anode, Figure 16 (C), has broadened and the oscillations on the reverse scan have diminished significantly. The second peak, Figure 16 (C), is not as broad as that obtained for the 1.0% Se anode, Figure 8 (C), but closely resembles that of the 1.0% O anode, Figure 11 (C). The second peak for the Kidd Creek anode, Figure 17 (C), is quite similar to that observed for the HBMS anode although the Kidd Creek anode contains more Se. The Kidd Creek anode also contains $\sim$0.17% Ag, Table 2, but the anode does not behave like the 0.1% Ag + 0.1% Se anode, Figures 12 and 13. The high O content of the commercial anodes could be playing a dominant role in this case.

The second peak for the CCR anode, Figure 18 (C), is very similar to that obtained for the 1.0% Ag anode, Figure 6 (C). Thus, the high Ag content, $\sim$0.3%, may be the dominant factor for this anode with respect to the shape of the CV curves. The commercial anodes contain various concentrations of Pb, Table 2, and the effect of increasing Pb

concentration on the anodic dissolution of synthetic copper electrodes will be the subject of another report.

A common feature of the cyclic voltammograms obtained in this study (Figures 3-18) is that they display a maximum current $I_{(max)}$; i.e., the first peak. $I_{(max)}$ usually decreases with continuous cycling due to the formation and accumulation of reaction products that adhere to the surface. In the case of pure copper, after a certain number of cycles, the product layer, Cu powder, loosens and flakes from the surface. This results in an increase in $I_{(max)}$ for the next cycle. In the case of the 1.0% Ag anode, the surface layer, ultimately silver powder, does not flake from the surface, but continues to grow, leading to the formation of a second peak in the CV.

Another feature of these cyclic voltammograms is that a hysteresis occurs for most anodes during the reverse scan. This hysteresis tends to broaden with time due to the accumulation of reaction products on the surface. The broadening of the hysteresis is related to the decrease in $I_{(max)}$. For anodes such as pure copper, where the reaction products loosens and flakes from the surface, the hysteresis on the ensuring cycle narrows and $I_{(max)}$ increases.

For certain anodes that establish a stable surface layer the hysteresis continues to broaden with continuous cycling and eventually a second peak forms. This second peak features a current minimum, $I_{(min)}$, and the shape of this peak is dependent on the type and concentration of impurity contained in the anode. For the silver bearing anodes, the second peak features a sharp $I_{(min)}$, that for the O-containing anodes is rounded, whereas the Se-anodes have a broad, flat $I_{(min)}$. The shape of the second peak may be due to changes in the composition of the accumulating reaction products on the anode surface. For example, in the case of the Ag-bearing anode, dissolved Ag^+ seems to be precipitated as Ag powder by the

locally high concentrations of Cu^+ at the corroding copper surface (3), according to:

$$Ag^+ + Cu^+ \rightarrow Ag^0 + Cu^{2+} \quad (1)$$

For anodes containing Se, the reactions occurring during the formation of the second peak probably involve the oxidation of Cu_2Se to form metal-deficient selenides (3) as follows:

$$Cu_2Se + x/2\ O_2 + xH_2SO_4 \rightarrow Cu_{2-x}Se + xCuSO_4 + xH_2O \quad (2)$$

$$2Cu_{2-x}Se + \frac{(1-2x)}{2}O_2 + (1-2x)H_2SO_4 \rightarrow Cu_3Se_2 + (1-2x)CuSO_4 + (1-2x)H_2O \quad (3)$$

$$1/2\ Cu_3Se_2 + \frac{(0.5-x)}{2}O_2 + (0.5-x)H_2SO_4 \rightarrow Cu_{1-x}Se + (0.5-x)CuSO_4 + (0.5-x)H_2O \quad (4)$$

$$Cu_{1-x}Se + \frac{x}{2}O_2 + xH_2SO_4 \rightarrow CuSe + xCuSO_4 + xH_2O \quad (5)$$

For copper anodes containing both Ag and Se impurities mineralogy studies of the anode slimes (3) suggest that reactions occurring during the formation of the second peak involve the silver enrichment of the selenides as follows:

$$Cu_2Se + xAg^+ \rightarrow (Cu_{2-x}Ag_x)Se + xCu^+ \quad (6)$$

$$(Cu_{2-x}Ag_x)Se + (1-x)Ag^+ \rightarrow AgCuSe + (1-x)Cu^+ \quad (7)$$

$$AgCuSe + (1-x)Ag^+ \rightarrow (Ag_{2-x}Cu_x)Se + (1-x)Cu^+ \quad (8)$$

$$(Ag_{2-x}Cu_x)Se + xAg^+ \rightarrow Ag_2Se + xCu^+ \quad (9)$$

Finally, the oscillations that often occur on the reverse scan of the CV cycle (and in certain cases during the forward scan) seem to be related to the "stability" of the layer formed on the anode surface. The more intense the oscillations, the less stable the surface layer. The absence of oscillations usually means that a very stable surface layer has formed. This is often the case when the anode contains a high concentration of impurity and forms a strong second peak; e.g., anodes containing 1.0% Ag, Se or O.

The results obtained in a previous study (1), indicated that a secondary electrochemically active surface was formed during the continuous cycling of the potential. This was confirmed by removing the "cycled" anodes, rinsing them, and in some cases, cleaning them very gently with a tissue. This procedure ensured the removal of much of the product layer without damaging the actual surface of the anode. The electrodes were then re-immersed in the electrolyte and the measurements continued. In the present study, all anodes were subjected to the above procedure after an initial 30 cycles. The difference between the CV profiles for a slime-covered and a cleaned surface was significant. Figures 19-21 show the CV profiles for Cu anodes containing 0.1% O, Ag and Se, respectively, that were taken (A) at the 30th cycle and (B) at the 1st cycle after cleaning. Partial elimination of the secondary surface (slimes layer) resulted in a dramatic increase in the anodic current and a complete change in the electrochemical profile of the anode.

The surface of a corroded anode which had been previously cleaned does not produce the second peak as quickly as a freshly polished surface. For example, Figure 22 shows the CV profile obtained after 66 cycles; i.e., 36 cycles after cleaning the surface. By comparing this profile to that in Figure 8 (C), it is readily seen that the second peak after 34 cycles on a cleaned surface is not as fully developed as that for a freshly polished surface after 23 cycles. This "surface conditioning" effect seems to depend on:

- the type and concentration of the impurities contained in the copper anode;
- the number of cycles that the electrode is subjected to; and
- the potential range used.

It is possible that the ease with which a particular copper anode forms the second peak is an indication of its tendency to passivate during electrorefining. Thus, by modifying the factors which cause the formation of the second peak it might be possible to reduce anode passivation; e.g., by employing an electrochemical pretreatment or conditioning technique. This hypothesis will be tested further by comparing potential-time profiles at constant current density for both treated and untreated anodes of similar composition.

To explore the hypothesis of a surface conditioning effect resulting from the continuous cycling of the anode potential, the cleaned surfaces of the various anodes were examined in the SEM to try to identify similarities in the surface morphologies. The procedure adopted was to remove the electrode from the cell after the final cycle, rinse the surface with distilled water and gently wipe the surface with a tissue. The results are presented in a series of SEM micrographs in Figures 23-35.

The corroded surfaces of most of the synthetic anodes, Figures 23-32, featured holes, and cavities (or depressions). Some of the cavities appeared to have an hexagonal shape as revealed at high magnification. These shapes may be cubo-octahedral holes resulting from the crystallographic dissolution of the fcc copper, the dissolution of Cu_2O crystal inclusions, or the release of a Cu_2Se spheroid. The surface morphologies for the pure copper anode

(Figure 23), the 0.1% Ag anode (Figure 24) and the 0.1% Se anode (Figures 25 and 26) are quite similar.

The corroded surfaces of the oxygen-containing anodes, although also featuring cubo-octahedral cavities, have a different morphology, Figures 27 and 28, than those of the pure Cu or Ag- and Se-containing anodes. In the case of the 0.1% O anode, the surface consists of "islands" of corroded Cu in a spongy copper matrix. Higher magnification, Figure 27, reveals that the "islands" contain cavities with hexagonal shapes as noted for the other anodes. The surface of the 1.0% O anode, Figure 28, displays a definite pattern of segments filled with holes of different shapes that likely represent chemical dissolution of the Cu_2O phase in the Cu-Cu_2O eutectic structure. At high magnification, the cubo-octahedral holes are also noted. The corroded surface of the 0.3% Ni +0.3%O anode, Figure 29, has a morphology very similar to that of the 0.1% O anode; cf., Figure 27.

Both the 1.0% Se- and 1.0% Ag-containing anodes, Figures 30 and 31, also have cubo-octahedral cavities in their corroded surfaces; furthermore, part of the slimes layer is still retained on the anode face. In the case of the Cu-1.0% Se anode, Figure 30, the pattern of the Cu_2Se inclusion network is clearly seen at low magnification. At high magnification the surface appears coarse (similar to that for pure Cu) and contains cubo-octahedral cavities and also partly liberated spheroids of Cu_2Se. The corroded surface of the Cu-1.0% Ag anode, Figure 31, is also coarse and retains a significant coverage of Ag powder.

The morphology of the corroded surface of the Cu-0.1% Ag + 0.1% Se anode is presented in Figure 32. The few cavities in the surface are not as clearly defined as those noted previously; the surface is coarse and contains both Ag powder and Cu_2Se spheroids.

The morphologies of the corroded commercial anodes are presented in Figures 33-35. The corroded surface of the HBMS anode, Figure 33, is very similar to that observed for the Cu-1.0% Se anode; cf., Figure 30. Several Cu_2Se spheroids in various states of liberation

are noted; some are within surface cavities caused by the rapid dissolution of the copper matrix around the inclusion.

The corroded surface of the Kidd Creek anode, Figure 34, is similar to that of the Cu-1.0% Se anode when viewed at low magnification. At high magnification, the surface is coarse and contains numerous holes of uniform size and shape. The holes result from the release of Cu_2Se spheroids. They are smaller than those observed for the synthetic and other commercial anodes because Kidd Creek employs a different casting procedure featuring more rapid cooling. The CCR anode, Figure 35, has a morphology similar to that observed for the Cu-0.1% Ag + 0.1% Se anode; cf., Figure 32. The surface is coarse with some cavities containing partially reacted Cu_2Se spheroids. Silver powder and Cu_2Se spheroids remain on the surface. Similar phases were noted by Dutrizac and Chen in their mineralogical studies on the anode slimes from the three Canadian Copper Refineries (2).

CONCLUSIONS

A reproducible technique using cyclic voltammetry has been developed to characterize the behaviour of impurity-containing copper anodes during electrorefining. The method involves cycling the anode potential at a rate of 2 mV/s between the open circuit potential of -0.35 V vs MSE and 0.0 V.

The type and concentration of the impurity contained in the copper anode produces characteristic and unique changes in the cyclic voltammograms obtained at a scan rate of 2 mV/s over the potential range E_r=-0.35 V vs MSE to +0.0 V. These changes include a decrease in the maximum current for copper dissolution (First Peak), a broadening of the hysteresis that occurs on the reverse scan, changes in the intensity of the oscillations that occur (mostly during the reverse scan) and the formation of a second peak featuring a minimum current. The shape of the second peak is related to the nature and composition of the product layer formed on the anode surface during the continuous cycling of the potential.

Removal of the slimes layer from the surface results in CV profiles that are significantly different than those obtained using a freshly polished surface. Specifically, the changes in the CV profiles mentioned above take longer to occur or do not occur at all. It appears that continuously cycling the potential has "conditioned" the anode surface such that the anode is, in some cases, less susceptible to passivation. There seems to be a definite connection between the CV profile exhibited by an anode and its tendency to passivate. Thus, the CV profiles of copper anodes containing variable concentrations of various impurities are being compiled, catalogued and extensively compared as it is highly probable that the passivation tendency of a commercial anode may be predicted by using this CV technique.

SEM examination of the "conditioned" surfaces of corroded anodes containing a variety of impurities shows that the surface morphologies are quite similar. Most of the corroded anode surfaces were coarse and also featured cavities having a cubo-octahedral shape. The surface morphologies of the various corroded anodes, however, showed subtle differences depending on the type and concentration of the impurities present.

REFERENCES

1. E.A. Kucharska-Giziewicz, "The behaviour of copper anodes with various impurity contents during electrorefining", MSL Divisional Report MSL 92-8 (TR), 1992.

2. J.E. Dutrizac and T.T. Chen, "A mineralogical comparison of the anode slimes from three Canadian copper refineries". Hydrometallurgy and Electrometallurgy of Copper, W.C. Cooper, G.E. Lugus and G. Ugarte, eds., University of Chile, Santiago, 467-486 (1987).

3. T.T. Chen and J.E. Dutrizac, "A mineralogical study of the deportment and reaction of silver during copper electrorefining", Metallurgical Transactions 20B (1989), 345-361.

Table 1 - Anodes Characterized by Cyclic Voltammetry and SEM/EDX Techniques in this Study

1. Pure Cu
2. Cu - 0.1% Ag
3. Cu - 0.1% Se
4. Cu - 0.1% O
5. Cu - 0.1% Ag + 0.1% Se
6. Cu - 1.0% Ag
7. Cu - 1.0% Se
8. Cu - 1.0% O
9. Cu - 0.3% Ni + 0.3% O
10. HBMS Commercial Anode
11. CCR Commercial Anode
12. Kidd Creek Commercial Anode

Table 2 - Typical Concentrations of Major Impurities Contained in the Commercial Anodes Used in this Study

Element	Percent In Anode		
	CCR	Kidd Creek	HBMS
Ag	0.29	0.17	-
Se	0.12	0.22	0.096
O	0.13-0.15	0.13-0.15	0.13-0.15
As	0.02-0.07	0.004	0.011
Pb	0.066	0.27	0.011

Figure Captions

Figure 1. Schematic drawing of the anode assembly.

Figure 2. Schematic drawing of the electrorefining cell.

Figure 3. Cyclic voltammograms showing the formation of peaks during the cycling of a Cu-0.1% Ag anode where: (1) 1st cycle, (2) 4th cycle and (3) 23rd cycle.

Figure 4. Cyclic voltammograms obtained for a pure copper anode: (A) 1st cycle, (B) 4th cycle and (C) 23rd cycle.

Figure 5. Cyclic voltammograms obtained for a Cu-0.1% Ag anode: (A) 1st cycle, (B) 8th cycle and (C) 23rd cycle.

Figure 6. Cyclic voltammograms obtained for a Cu-1.0% Ag anode: (A) 1st cycle, (B) 4th cycle and (C) 23rd cycle.

Figure 7. Cyclic voltammograms obtained for a Cu-0.1% Se anode: (A) 1st cycle, (B) 6th cycle and (C) 23rd cycle.

Figure 8. Cyclic voltammograms obtained for a Cu-1.0% Se anode: (A) 1st cycle, (B) 4th cycle and (C) 23rd cycle.

Figure 9. Cyclic voltammograms obtained for a Cu-0.1% O anode: (A) 1st cycle, (B) 6th cycle and (C) 23rd cycle.

Figure 10. Cyclic voltammograms obtained for a Cu-0.1% O anode: (A) 10th cycle, (B) 12th cycle and (C) 13th cycle.

Figure 11. Cyclic voltammograms obtained for a Cu-1.0% O anode: (A) 1st cycle, (B) 4th cycle and (C) 23rd cycle.

Figure 12. Cyclic voltammograms obtained for a Cu-0.1% Ag + 0.1 % Se anode: (A) 1st cycle, (B) 4th cycle and (C) 23rd cycle.

Figure 13. Cyclic voltammograms obtained for a Cu-0.1% Ag + 0.1% Se anode: (A) 6th cycle, (B) 9th cycle and (C) 16th cycle.

Figure 14. Cyclic voltammograms obtained for a Cu-0.3% Ni +0.3% O anode: (A) 1st cycle, (b) 6th cycle and (C) 23rd cycle.

Figure 15. Cyclic voltammograms obtained for a Cu-0.3% Ni +0.3% O anode: (A) 20th cycle, (B) 21st cycle and (C) 22nd cycle.

Figure 16. Cyclic voltammograms obtained for a HBMS commercial anode: (A) 1st cycle, (B) 6th cycle and (C) 23rd cycle.

Figure 17. Cyclic voltammograms obtained for a Kidd Creek commercial anode: (A) 1st cycle, (B) 6th cycle and (C) 23rd cycle.

Figure 18. Cyclic voltammograms obtained for a CCR commercial anode: (A) 1st cycle, (B) 7th cycle and (C) 23rd cycle.

Figure 19. Cyclic voltammograms obtained for a Cu-0.1% O anode: (A) 30th cycle and (B) 1st cycle after cleaning the surface.

Figure 20. Cyclic voltammograms obtained for a Cu-0.1% Ag anode: (A) 30th cycle and (B) 1st cycle after cleaning the surface.

Figure 21. Cyclic voltammograms obtained for a Cu-0.1% Se anode: (A) 30th cycle and (B) 1st cycle after cleaning the surface.

Figure 22. Cyclic voltammograms obtained for a Cu-1.0% Se anode showing the last (66th) cycle prior to SEM observation.

Figure 23. SE micrographs showing the morphology of the cleaned surface of a pure copper anode after 40 cycles.

Figure 24. SE micrographs showing the morphology of the cleaned surface of a Cu-0.1% Ag anode after 31 cycles.

Figure 25. SE micrographs showing the morphology of the cleaned surface of a Cu-0.1% Se anode after 31 cycles.

Figures 26. SE micrographs showing the morphology of the cleaned surface of a Cu-0.1% Se anode after 60 cycles.

Figure 27. SE micrographs showing the morphology of the cleaned surface of a Cu-0.1% O anode after 31 cycles.

Figure 28. SE micrographs showing the morphology of the cleaned surface of a Cu-1.0% O anode after 36 cycles.

Figure 29. SE micrographs showing the morphology of the cleaned surface of a Cu-0.3% Ni +0.3% O anode after 27 cycles.

Figure 30. SE micrographs showing the morphology of the cleaned surface of a Cu-1.0% Se anode after 66 cycles. Rounded white particles are Cu_2Se spheroids.

Figure 31. SE micrographs showing the morphology of the cleaned surface of a Cu-1.0% Ag anode after 30 cycles. White clusters are Ag powder.

Figure 32. SE micrographs showing the morphology of the cleaned surface of a Cu-0.1% Ag + 0.1% Se anode after 47 cycles. Rounded particles are Cu_2Se spheroids.

Figure 33. SE micrographs showing the morphology of the cleaned surface of a HBMS commercial anode after 32 cycles. Rounded particles are Cu_2Se spheroids.

Figure 34. SE micrographs showing the morphology of the cleaned surface of a Kidd Creek commercial anode after 39 cycles. Holes are due to the release of Cu_2Se spheroids.

Figure 35. SE micrographs showing the morphology of the cleaned surface of a CCR commercial anode after 55 cycles. Rounded particles are Cu_2Se spheroids and the white clusters are Ag powder.

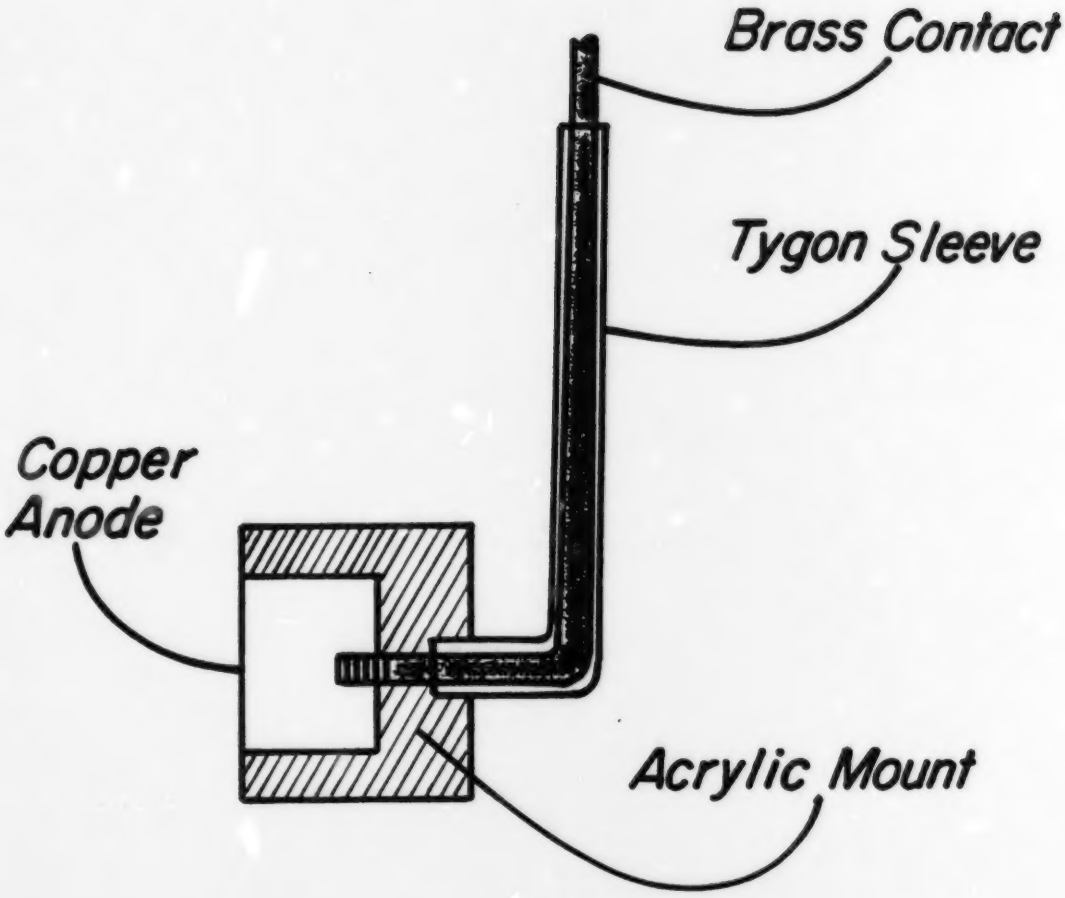

Figure 1. Schematic drawing of the anode assembly.

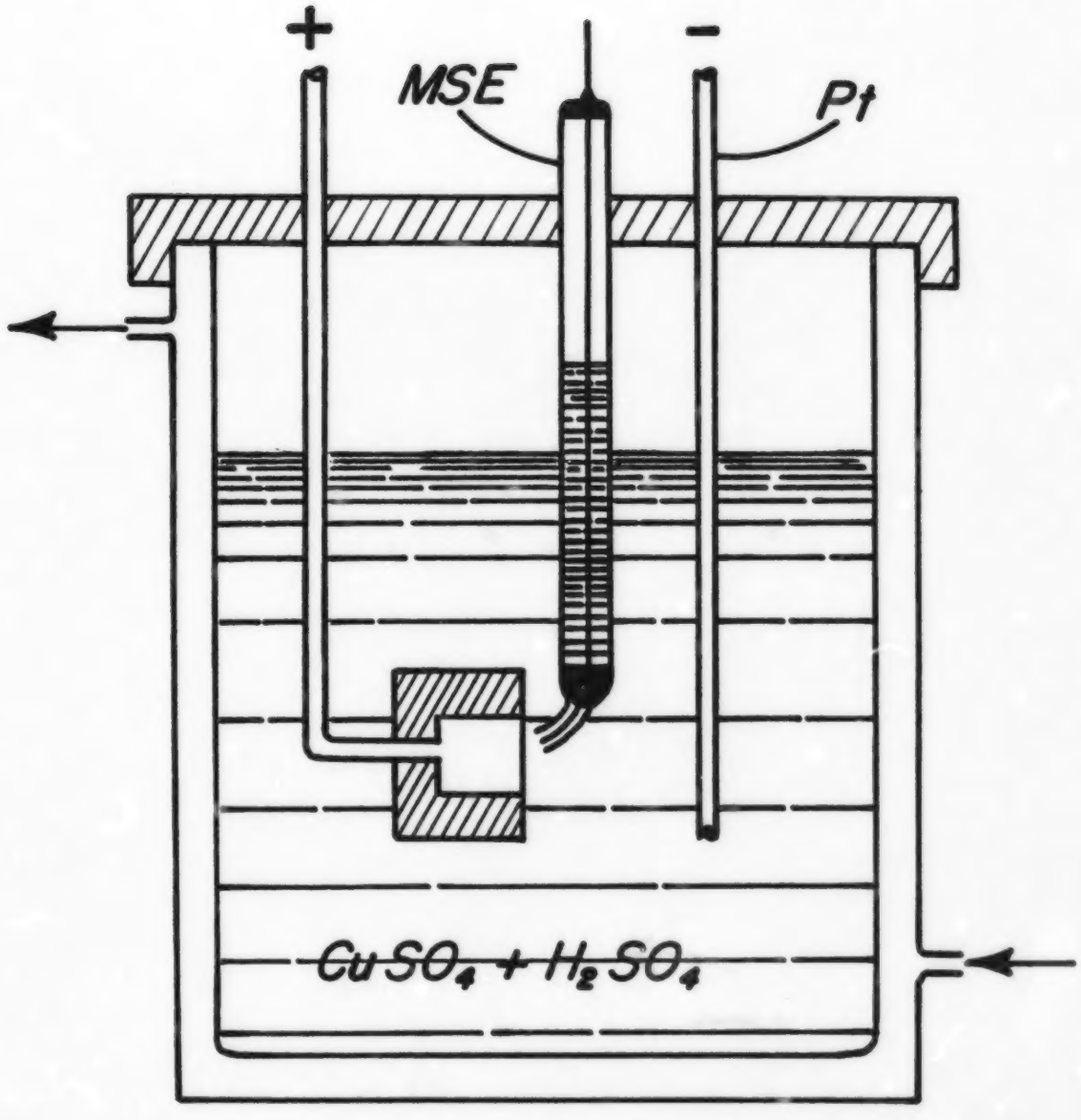

Figure 2. Schematic drawing of the electrorefining cell.

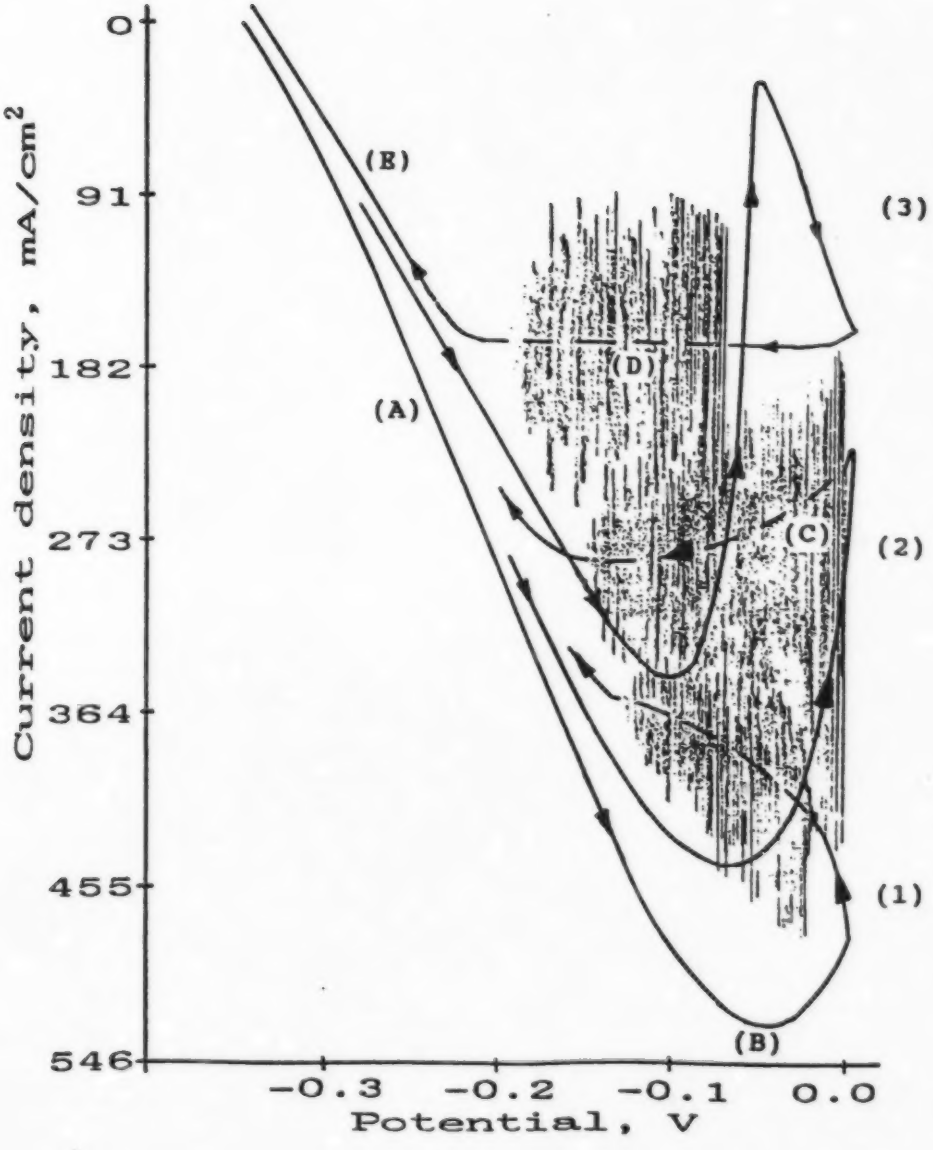

Figure 3. Cyclic voltammograms showing the formation of peaks during the cycling of a Cu-0.1% Ag anode where: (1) 1st cycle, (2) 4th cycle and (3) 23rd cycle.

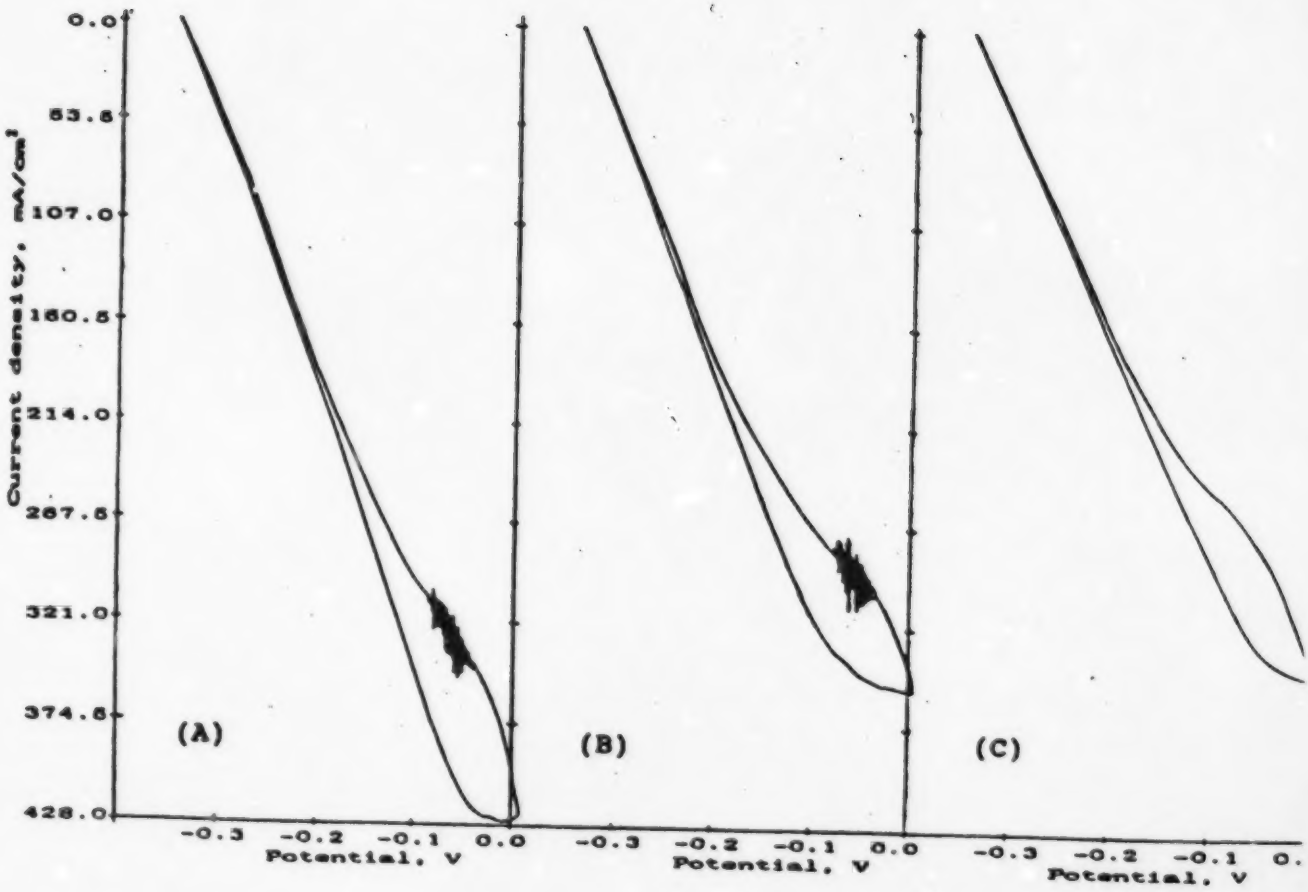

Figure 4. Cyclic voltammograms obtained for a pure copper anode: (A) 1st cycle, (B) 4th cycle and (C) 23rd cycle.

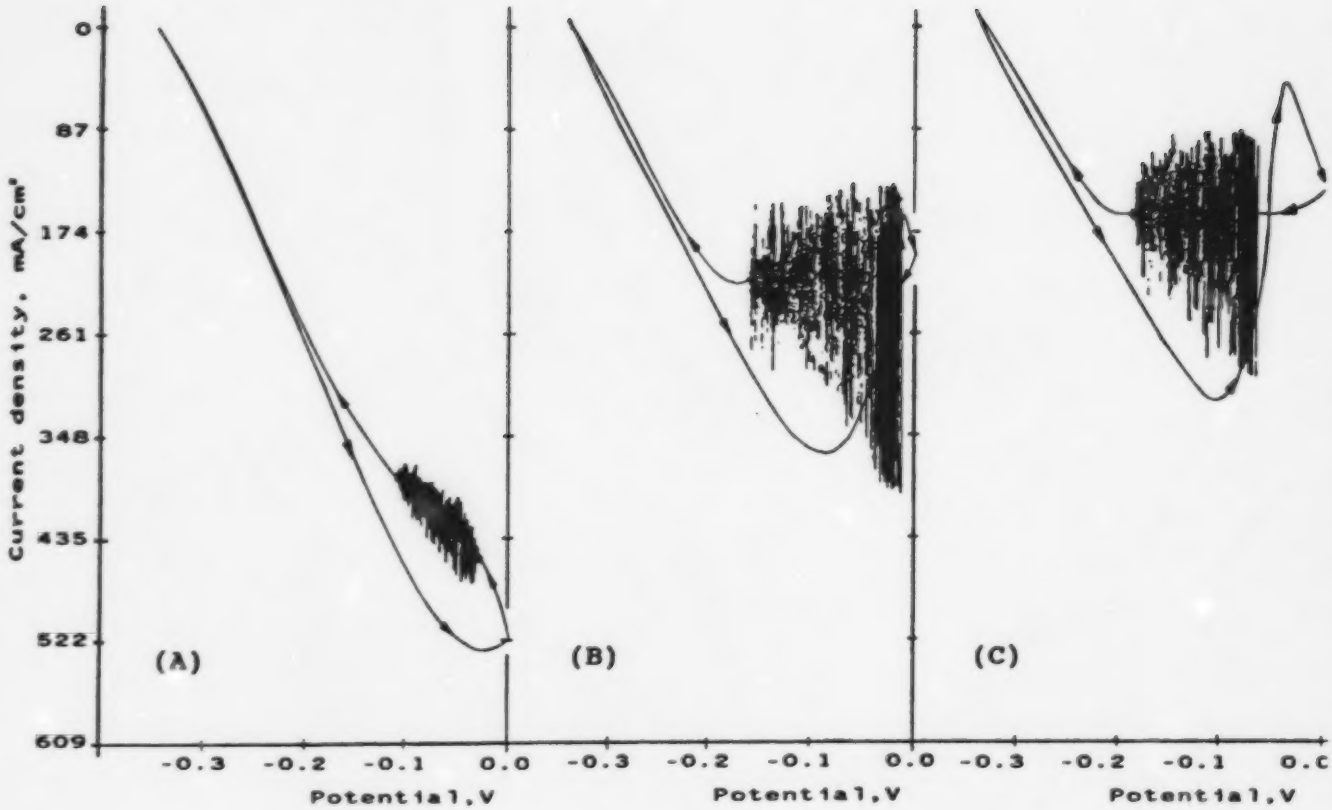

Figure 5. Cyclic voltammograms obtained for a Cu-0.1% Ag anode: (A) 1st cycle, (B) 8th cycle and (C) 23rd cycle.

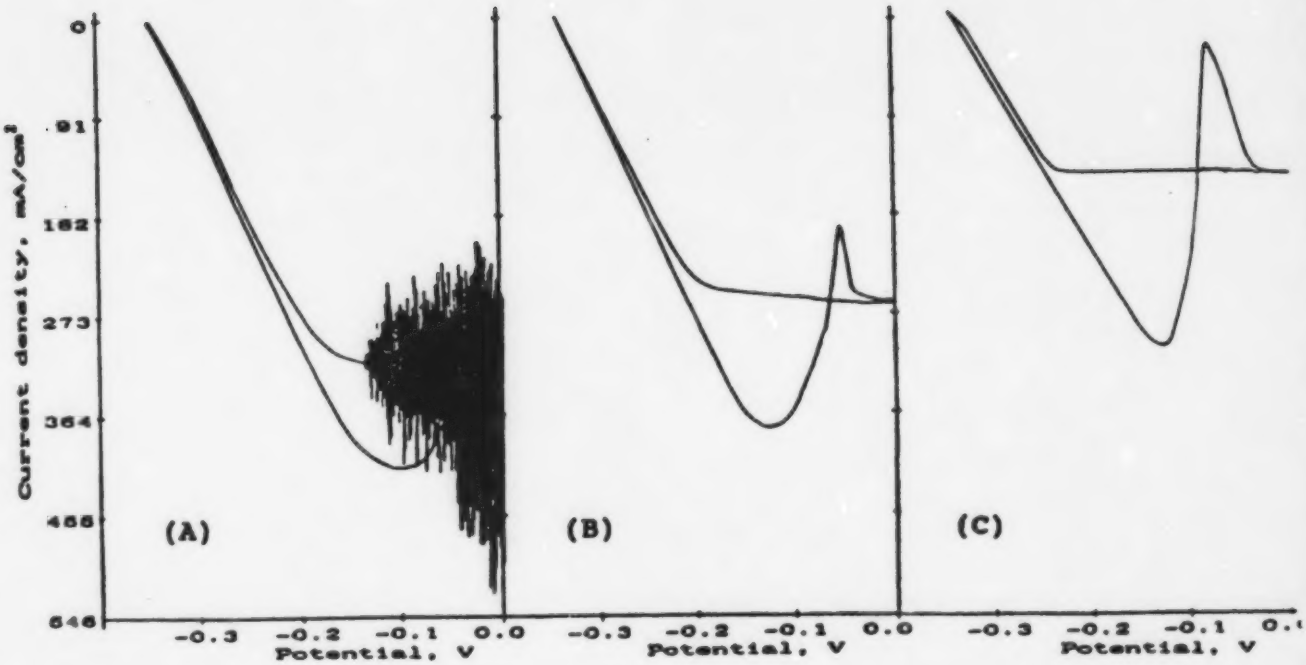

Figure 6. Cyclic voltammograms obtained for a Cu-1.0% Ag anode: (A) 1st cycle, (B) 4th cycle and (C) 23rd cycle.

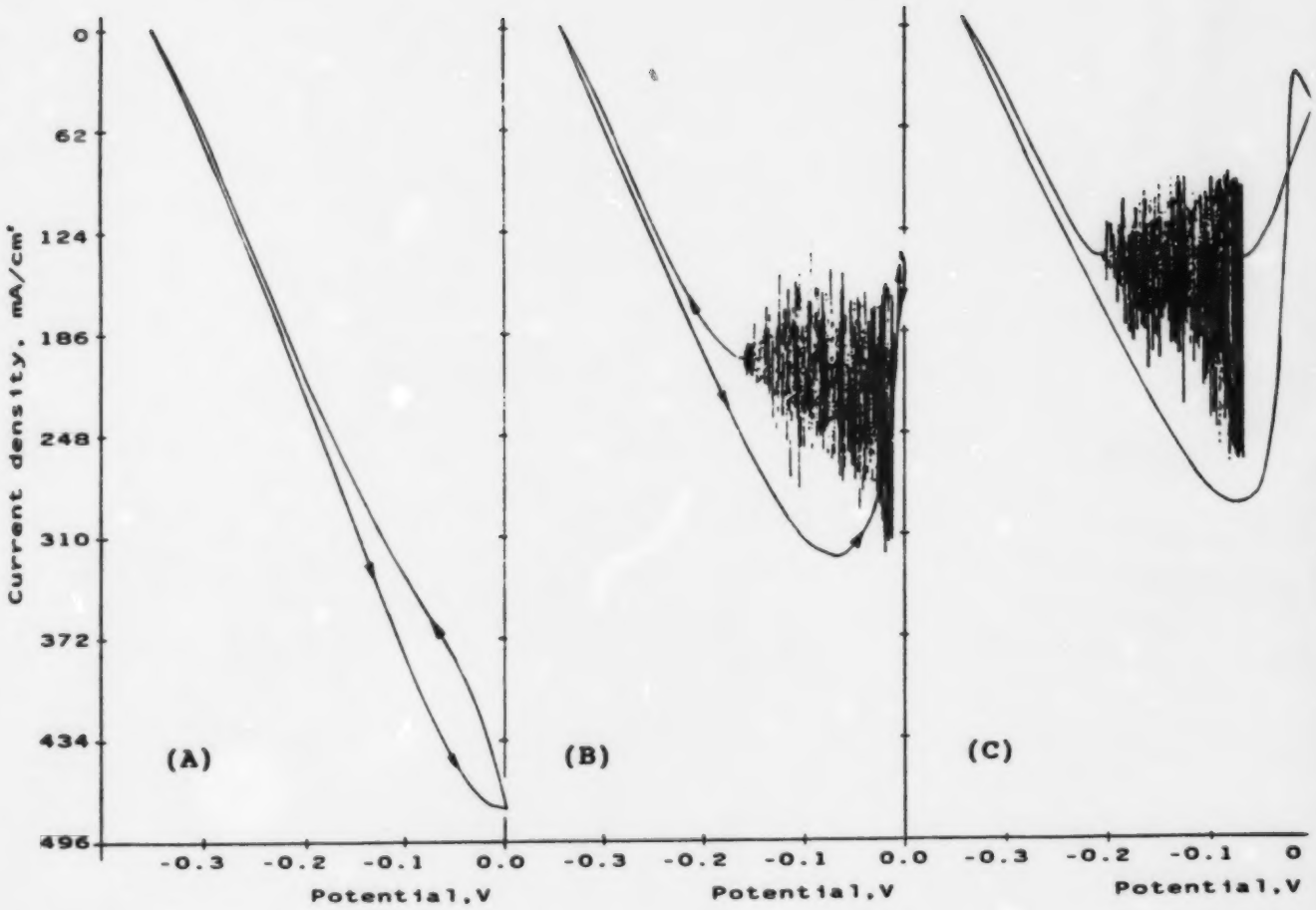

Figure 7. Cyclic voltammograms obtained for a Cu-0.1% Se anode: (A) 1st cycle, (B) 6th cycle and (C) 23rd cycle.

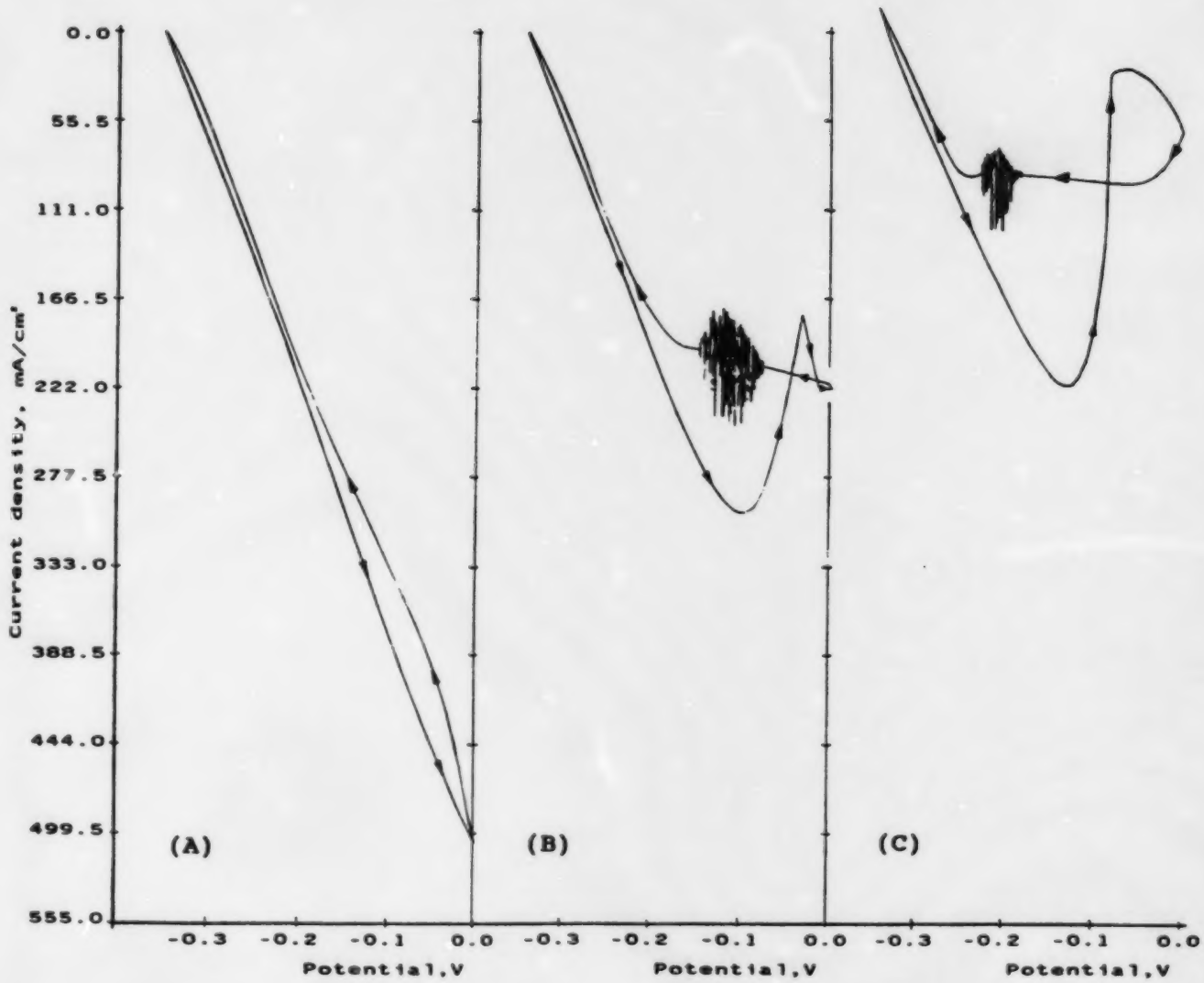

Figure 8. Cyclic voltammograms obtained for a Cu-1.0% Se anode: (A) 1st cycle, (B) 4th cycle and (C) 23rd cycle.

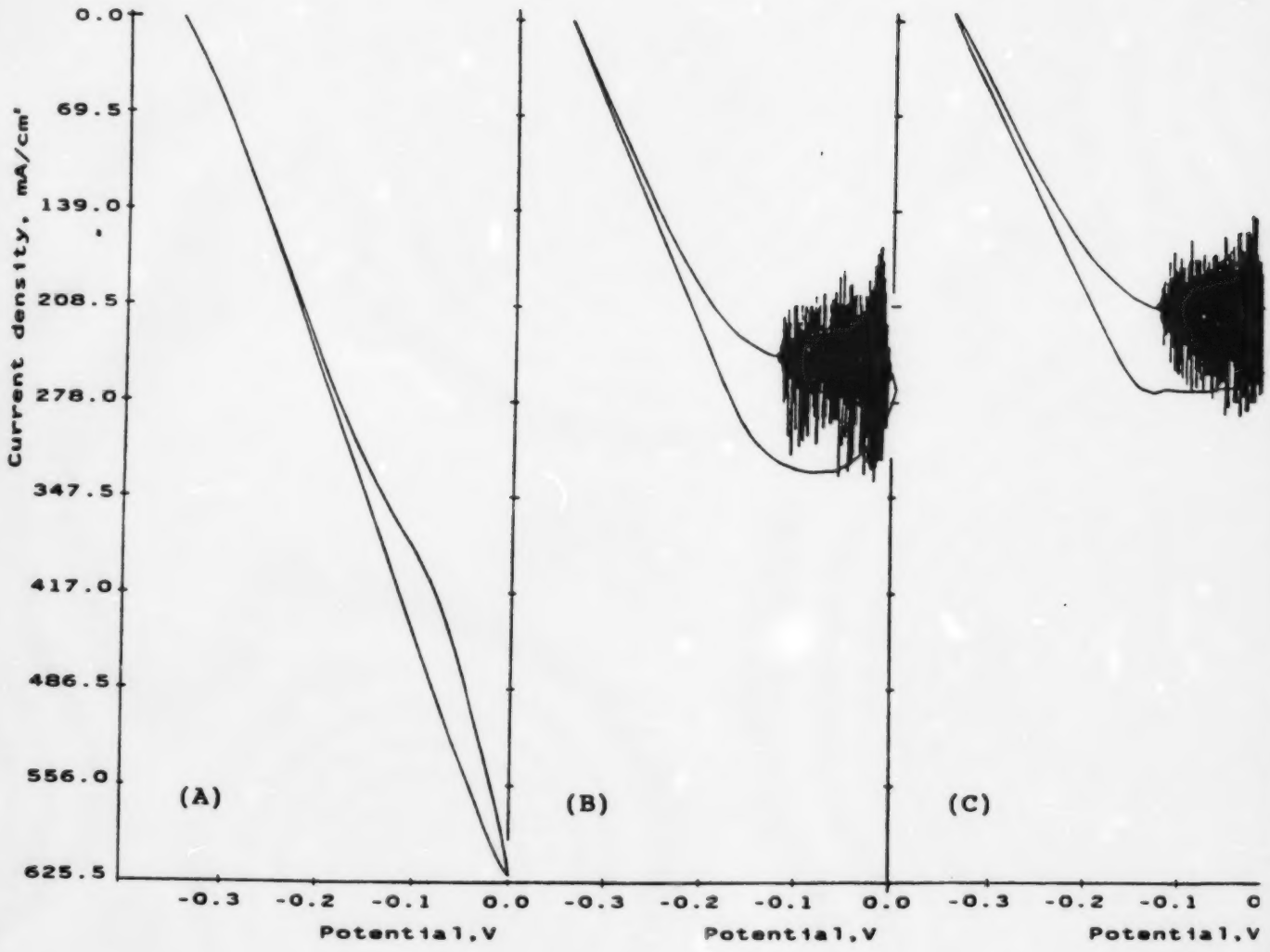

Figure 9. Cyclic voltammograms obtained for a Cu-0.1% O anode: (A) 1st cycle, (B) 6th cycle and (C) 23rd cycle.

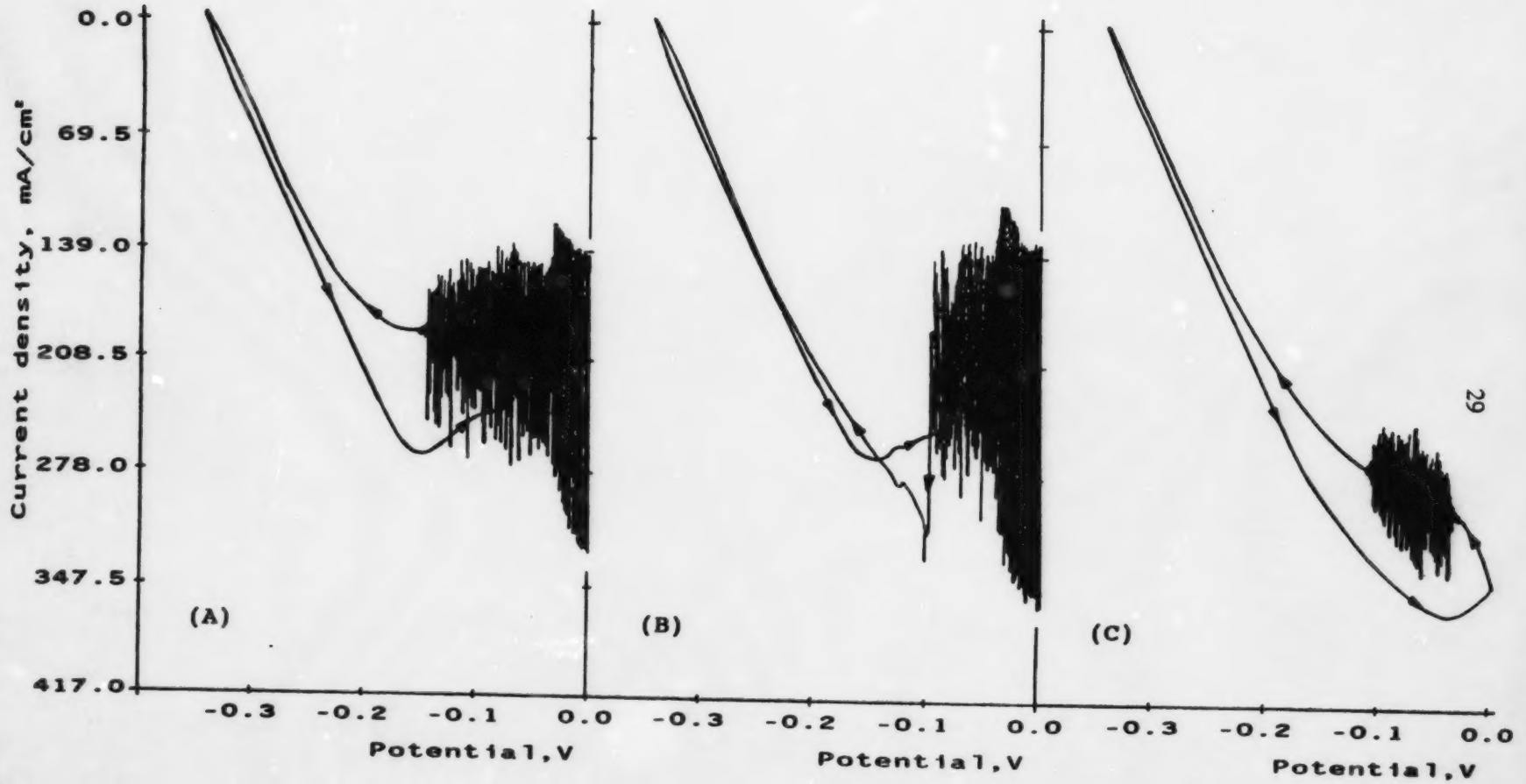

Figure 10. Cyclic voltammograms obtained for a Cu-0.1% O anode: (A) 10th cycle, (B) 12th cycle and (C) 13th cycle.

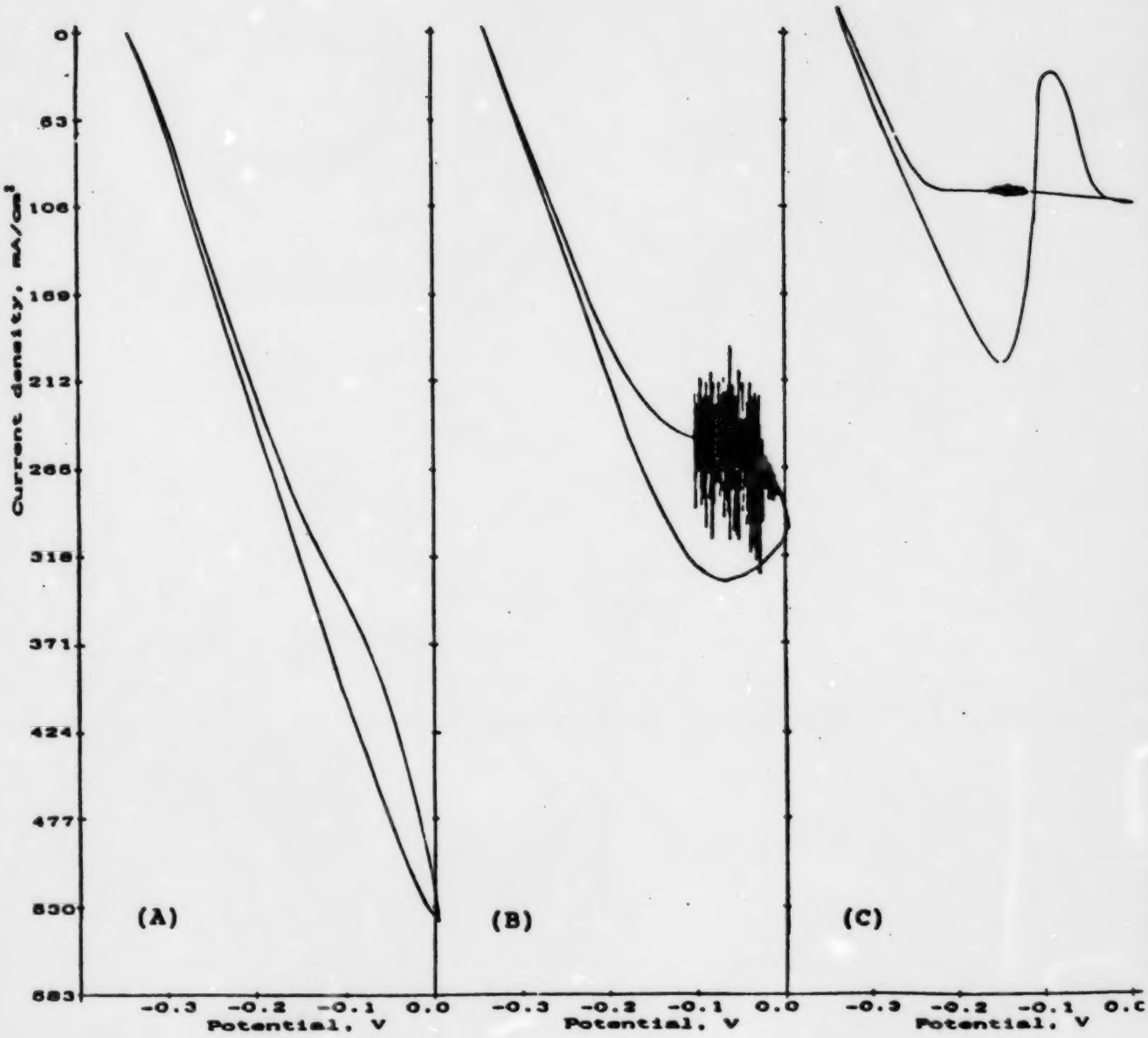

Figure 11. Cyclic voltammograms obtained for a Cu-1.0% O anode: (A) 1st cycle, (B) 4th cycle and (C) 23rd cycle.

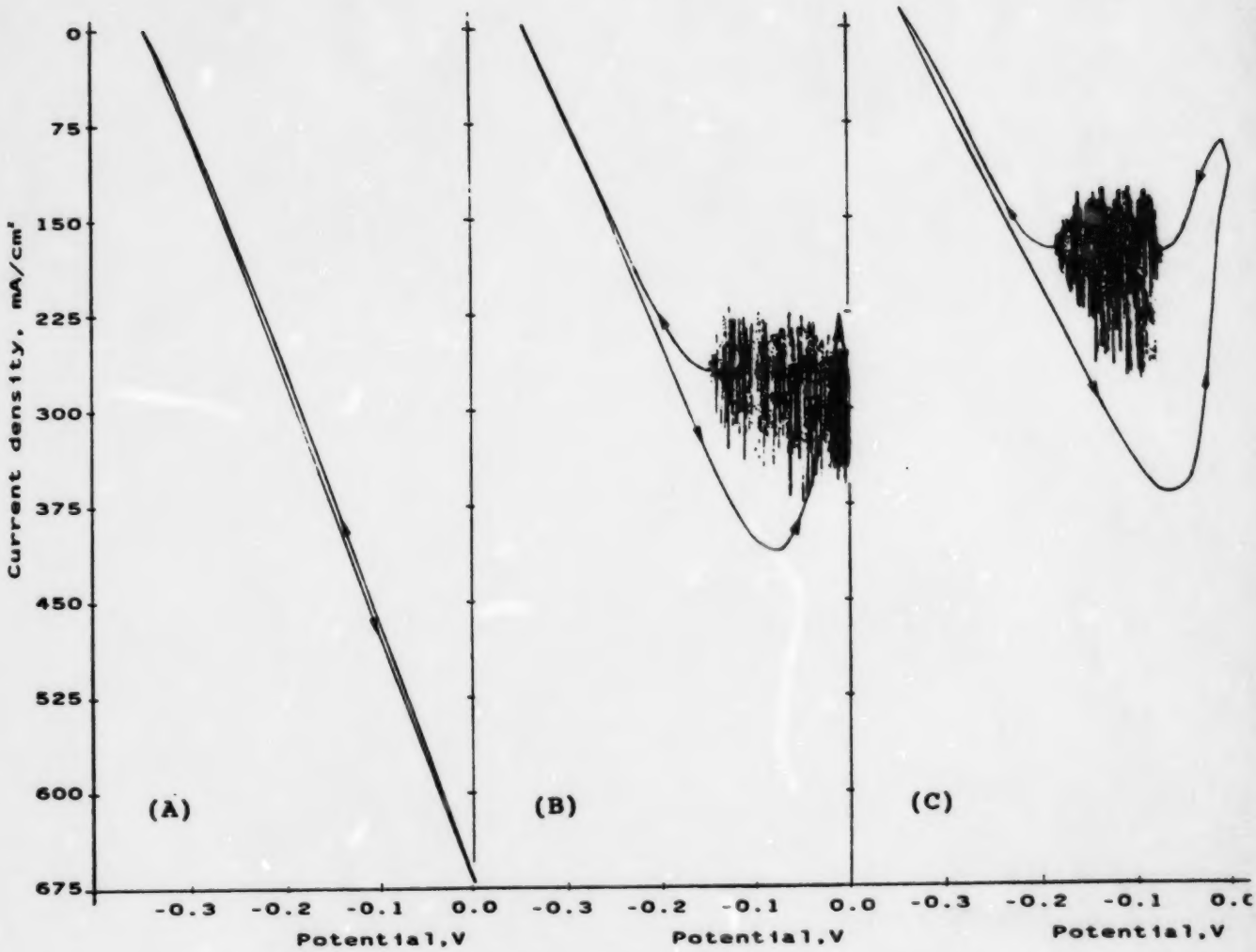

Figure 12. Cyclic voltammograms obtained for a Cu-0.1% Ag + 0.1 % Se anode: (A) 1st cycle, (B) 4th cycle and (C) 23rd cycle.

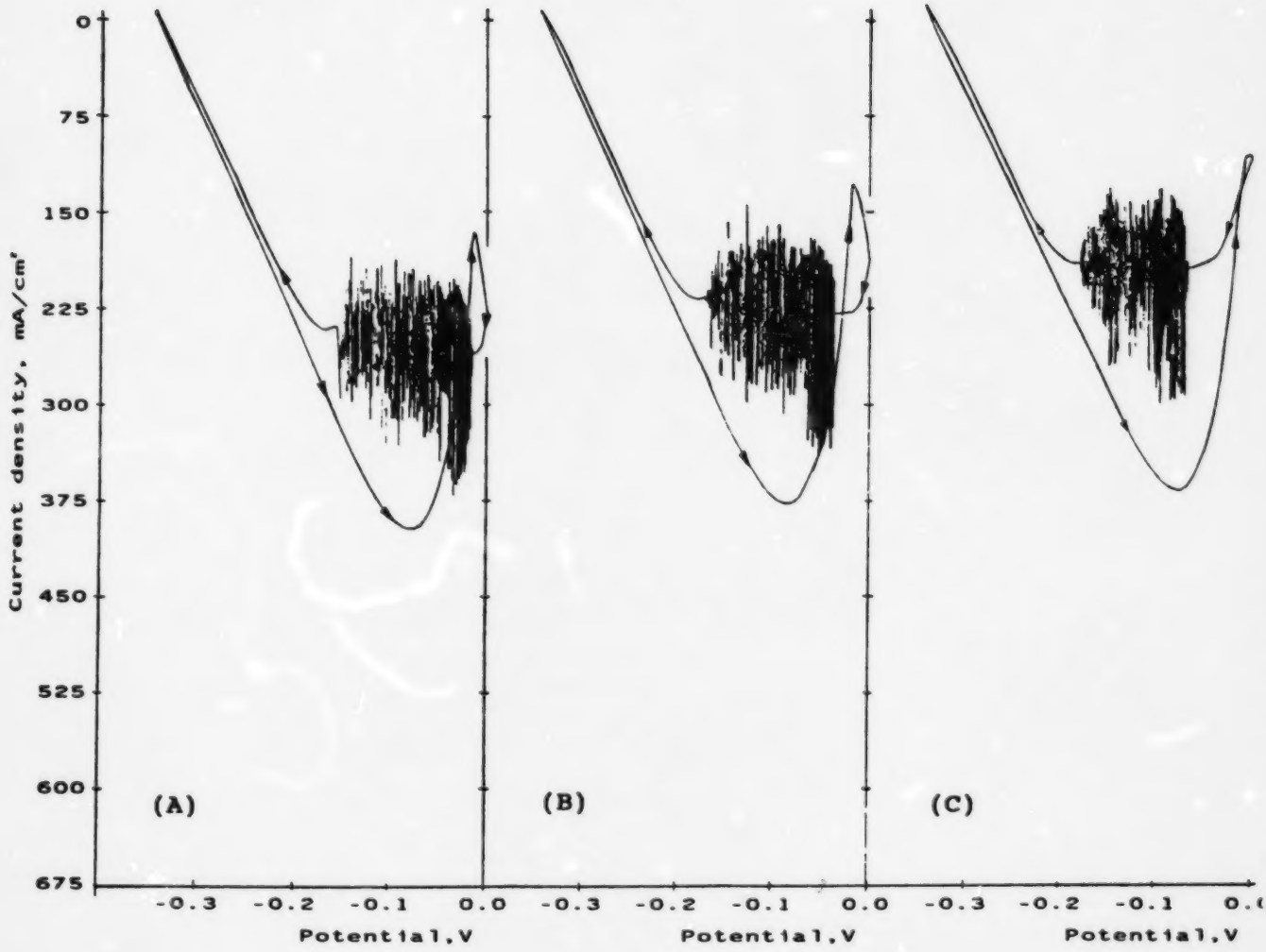

Figure 13. Cyclic voltammograms obtained for a Cu-0.1% Ag + 0.1% Se anode: (A) 6th cycle, (B) 9th cycle and (C) 16th cycle.

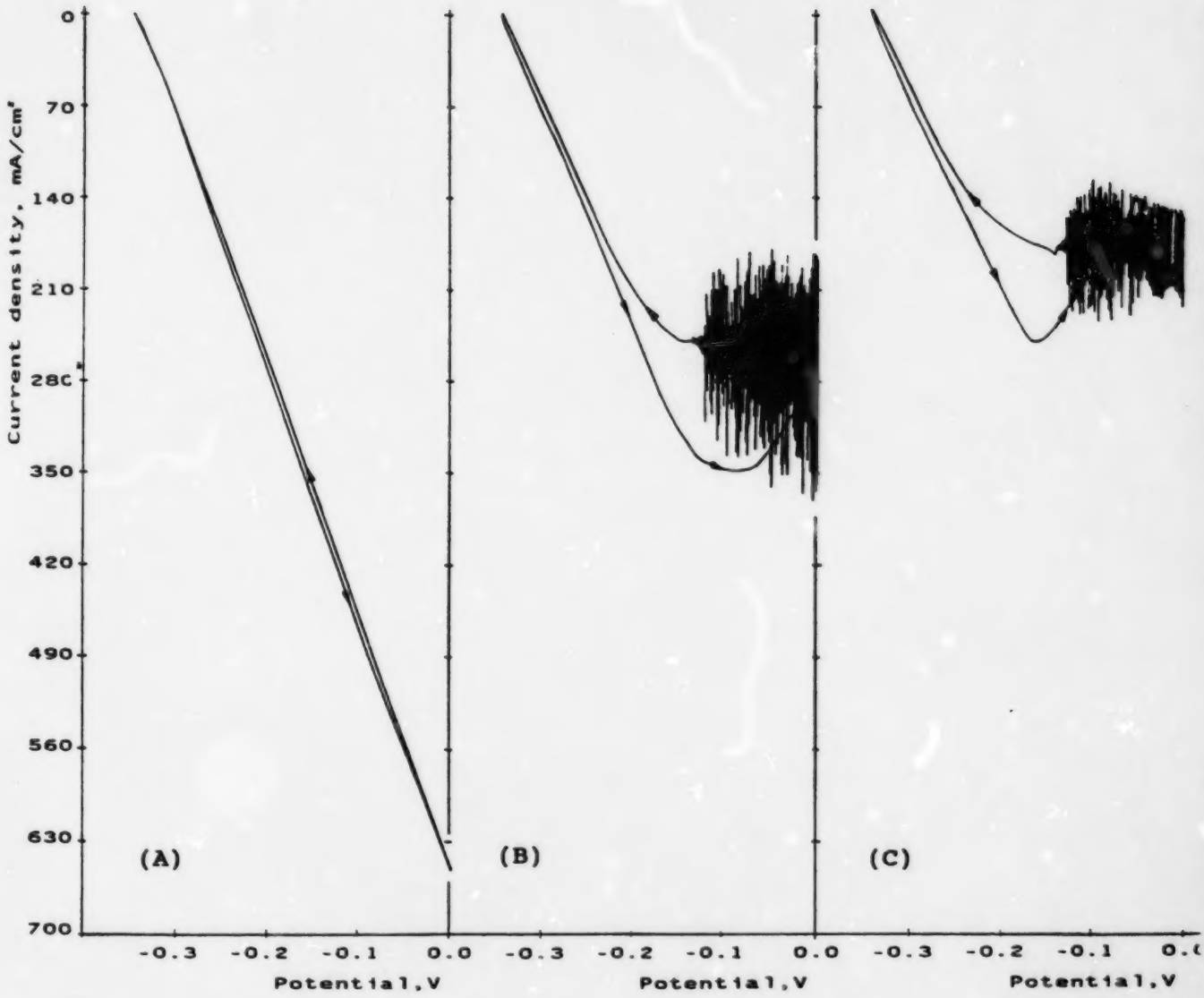

Figure 14. Cyclic voltammograms obtained for a Cu-0.3% Ni +0.3% O anode: (A) 1st cycle, (b) 6th cycle and (C) 23rd cycle.

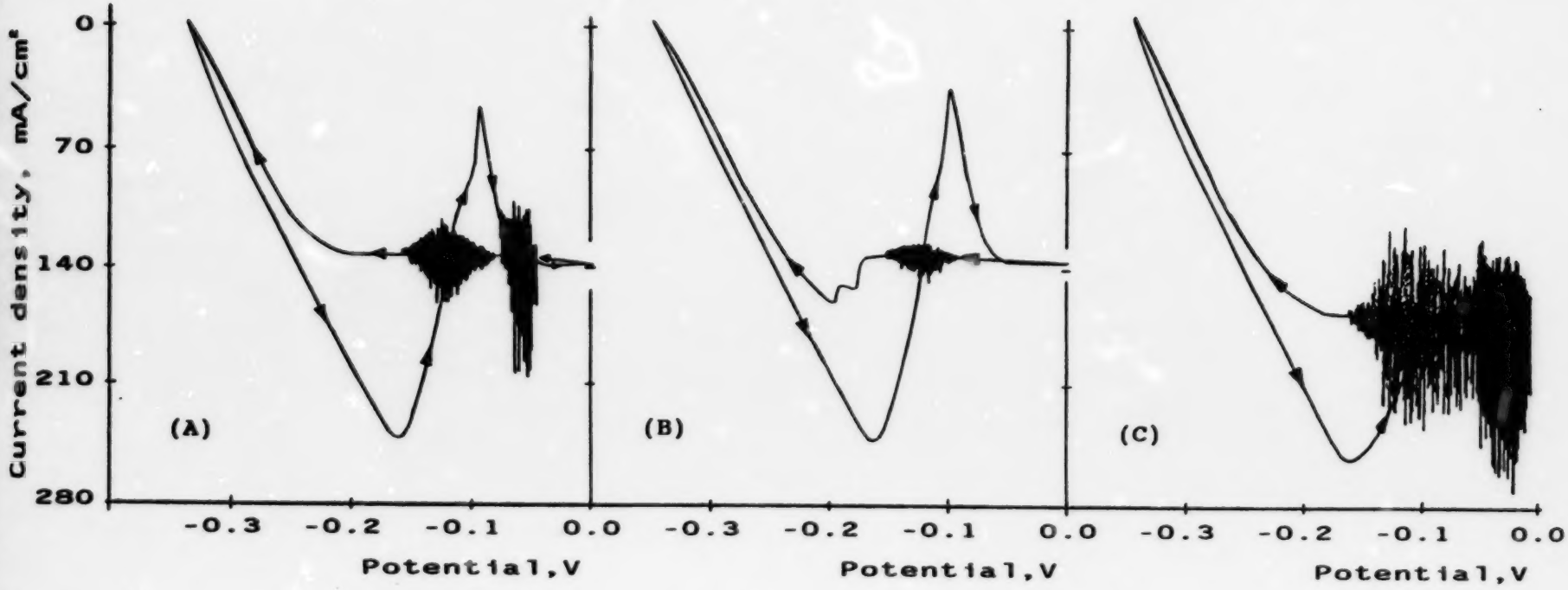

Figure 15. Cyclic voltammograms obtained for a Cu-0.3% Ni +0.3% O anode: (A) 20th cycle, (B) 21st cycle and (C) 22nd cycle.

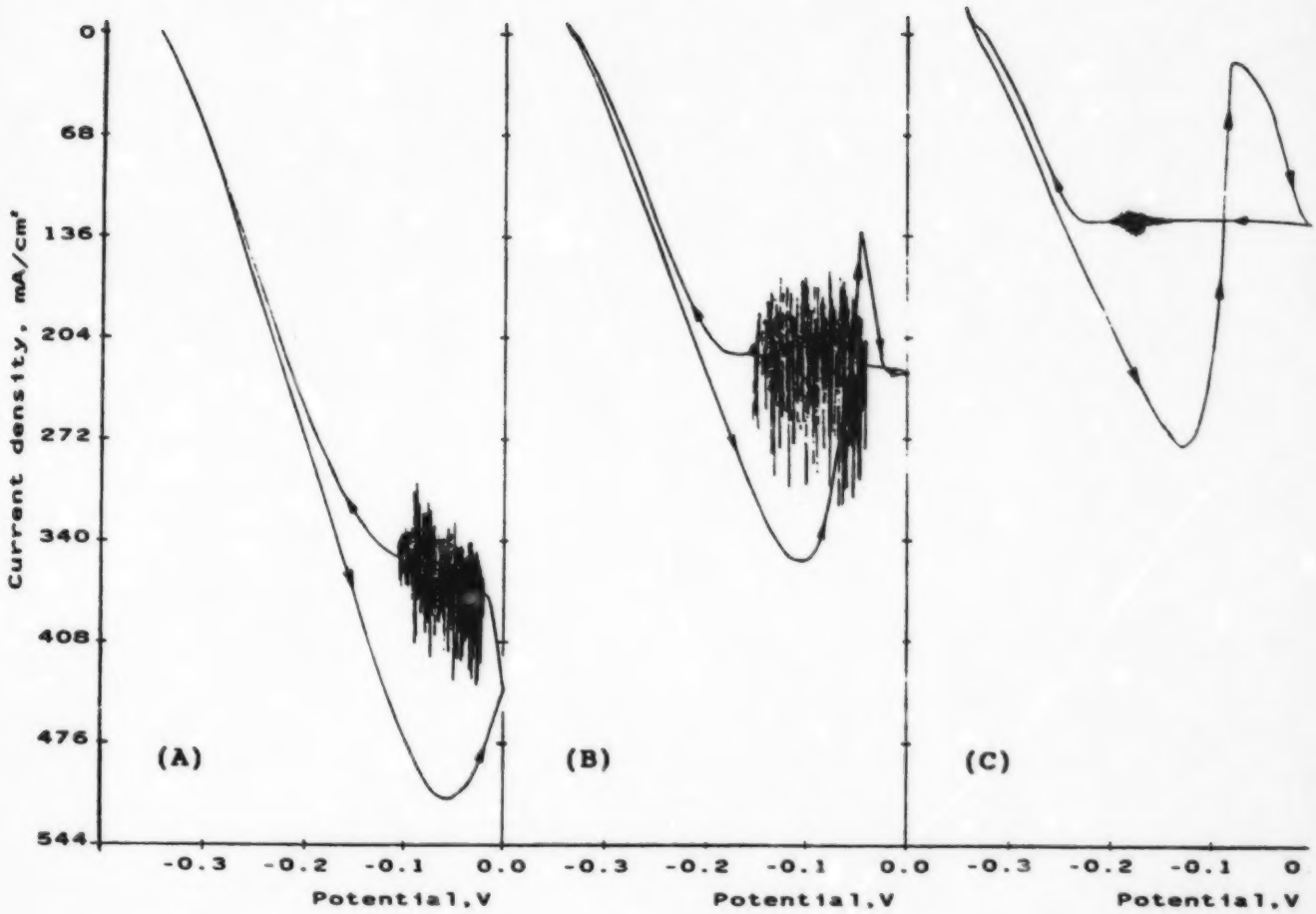

Figure 16. Cyclic voltammograms obtained for a HBMS commercial anode: (A) 1st cycle, (B) 6th cycle and (C) 23rd cycle.

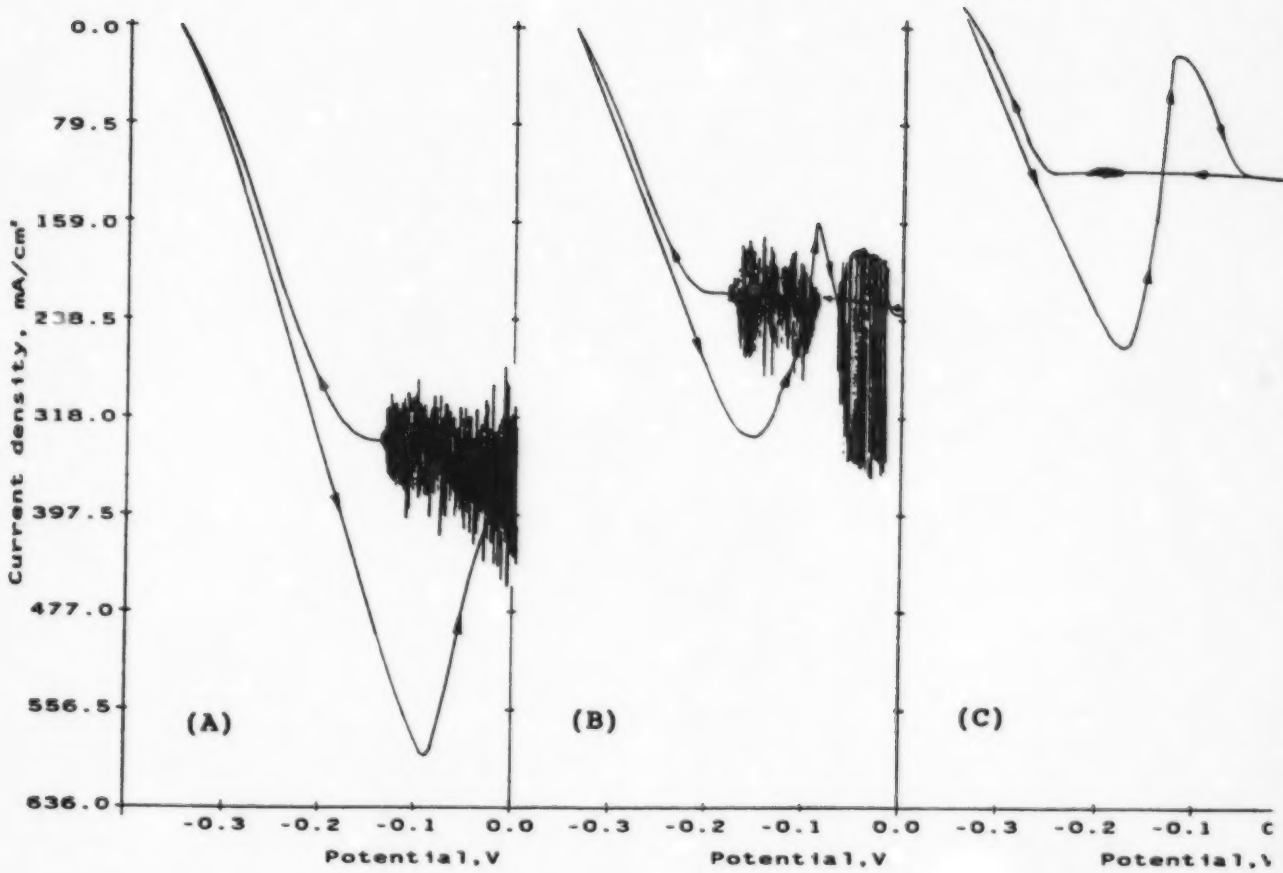

Figure 17. Cyclic voltammograms obtained for a Kidd Creek commercial anode: (A) 1st cycle, (B) 6th cycle and (C) 23rd cycle.

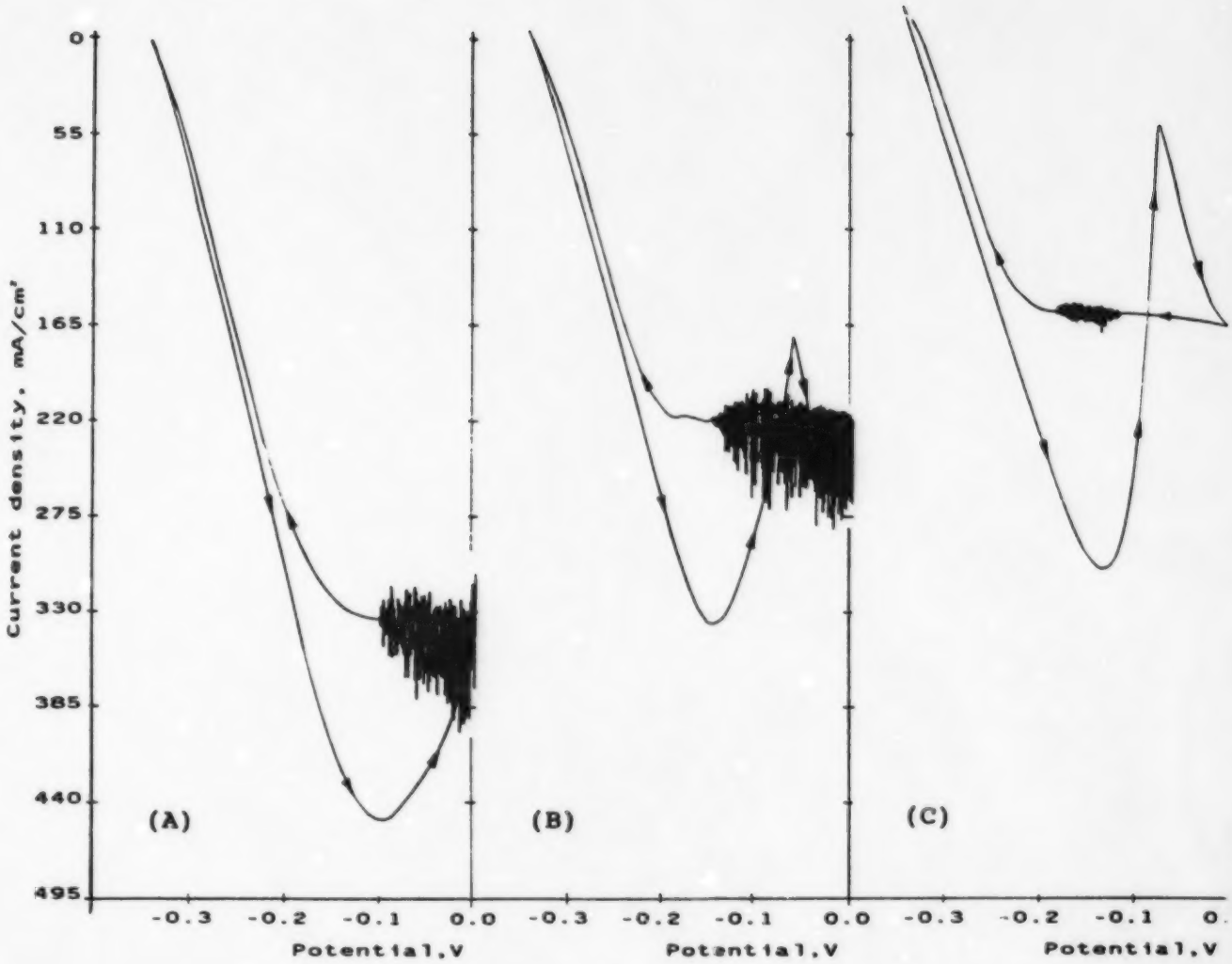

Figure 18. Cyclic voltammograms obtained for a CCR commercial anode: (A) 1st cycle, (B) 7th cycle and (C) 23rd cycle.

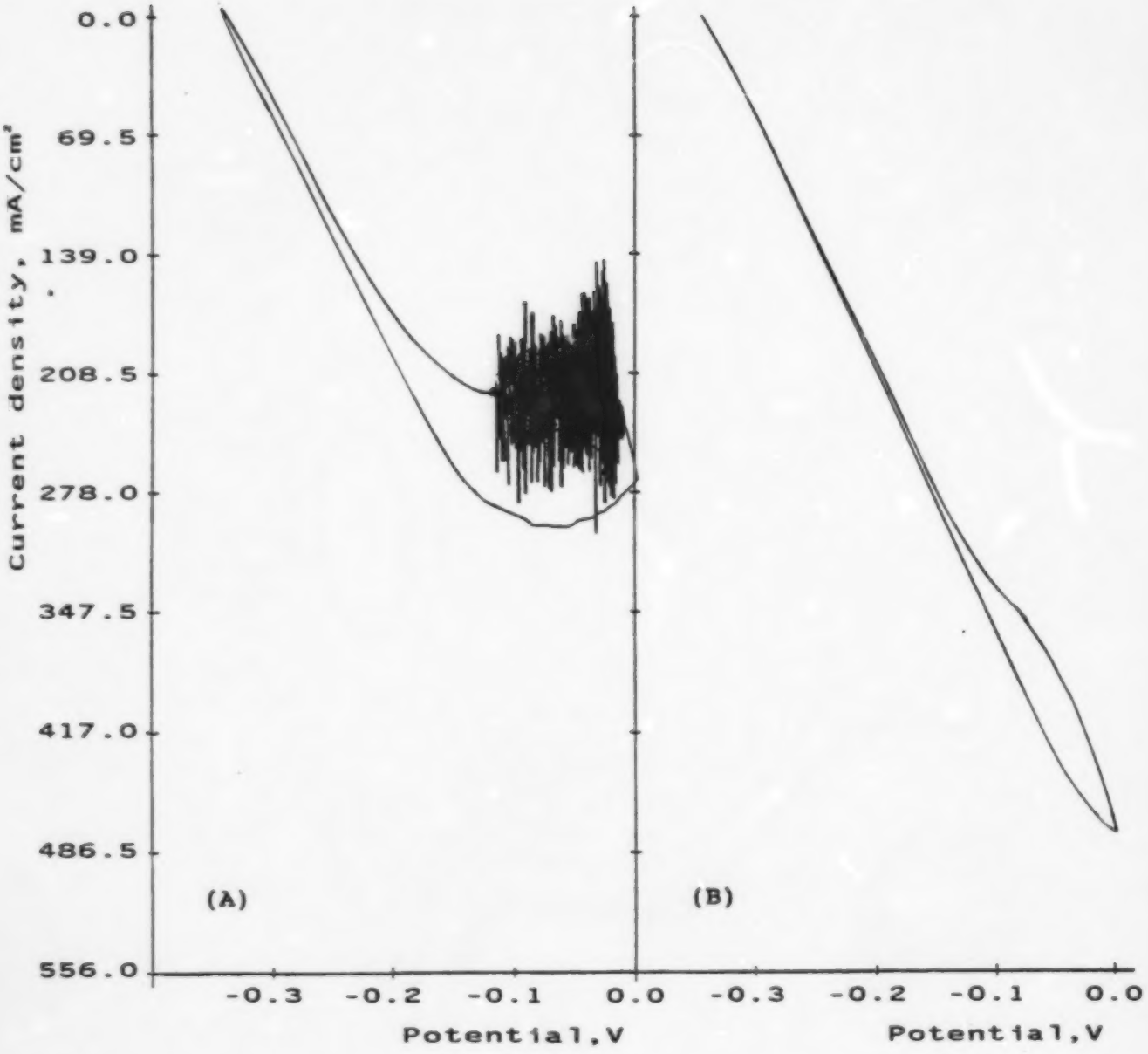

Figure 19. Cyclic voltammograms obtained for a Cu-0.1% O anode: (A) 30th cycle and (B) 1st cycle after cleaning the surface.

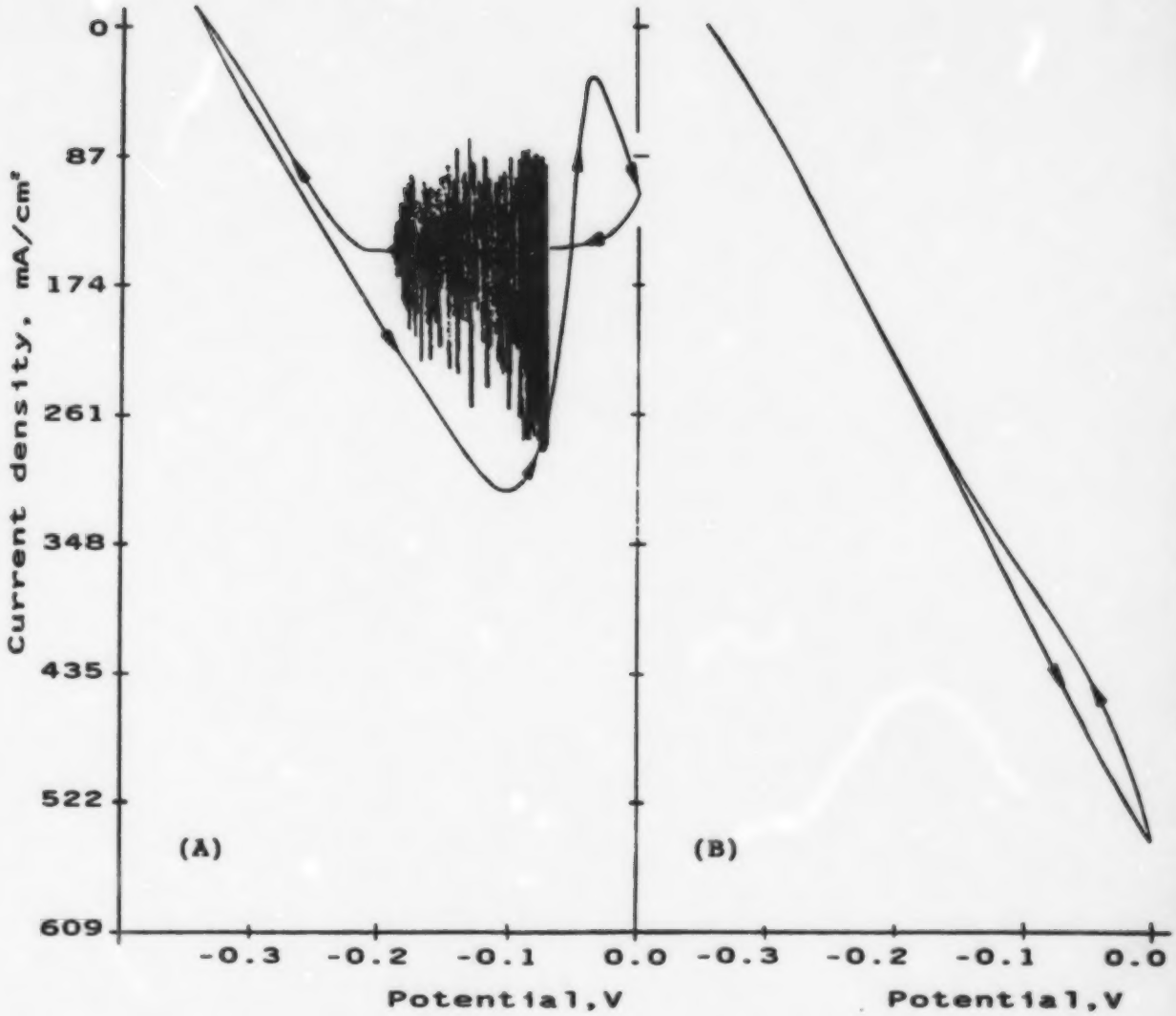

Figure 20. Cyclic voltammograms obtained for a Cu-0.1% Ag anode: (A) 30th cycle and (B) 1st cycle after cleaning the surface.

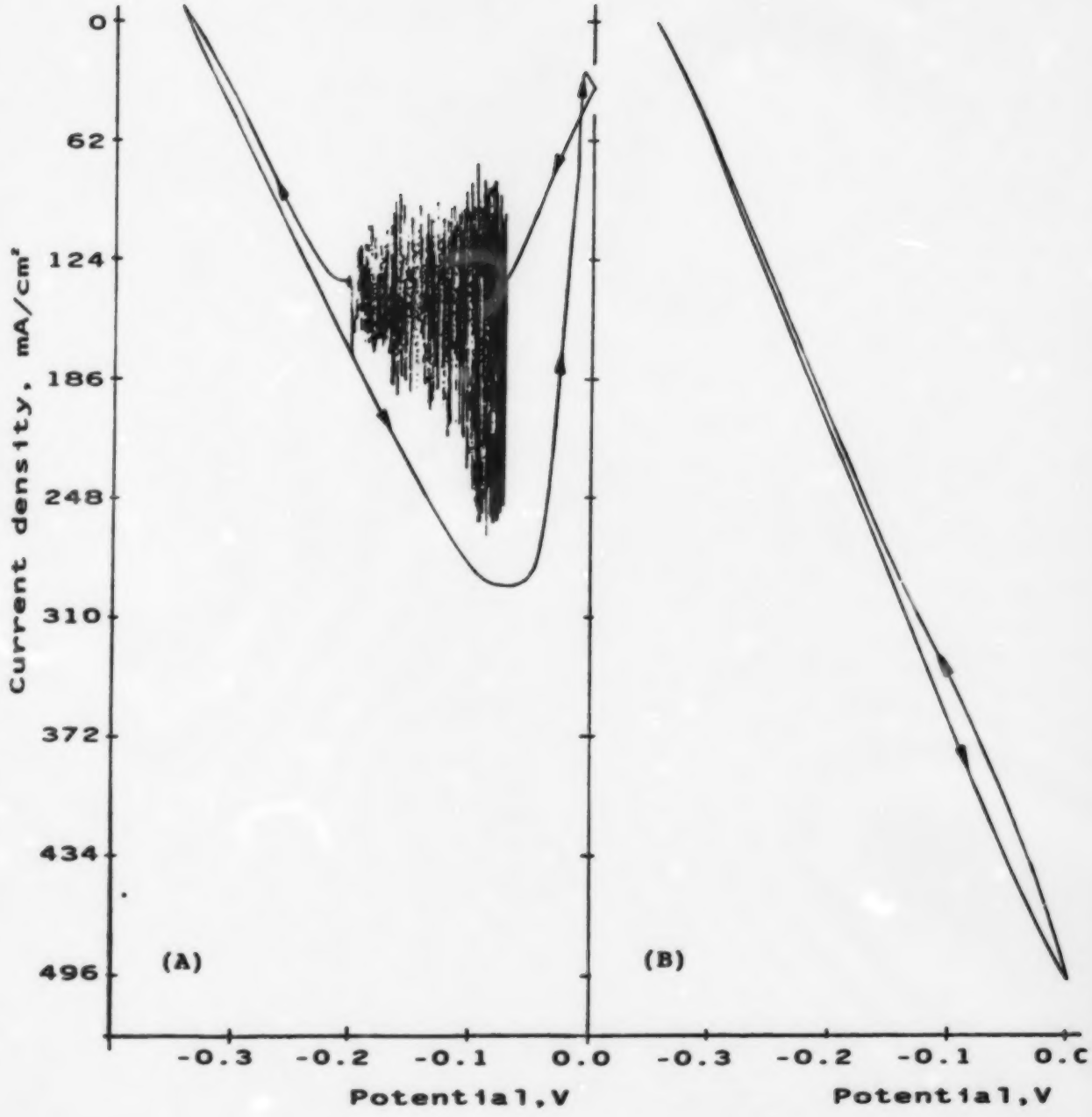

Figure 21. Cyclic voltammograms obtained for a Cu-0.1% Se anode: (A) 30th cycle and (B) 1st cycle after cleaning the surface.

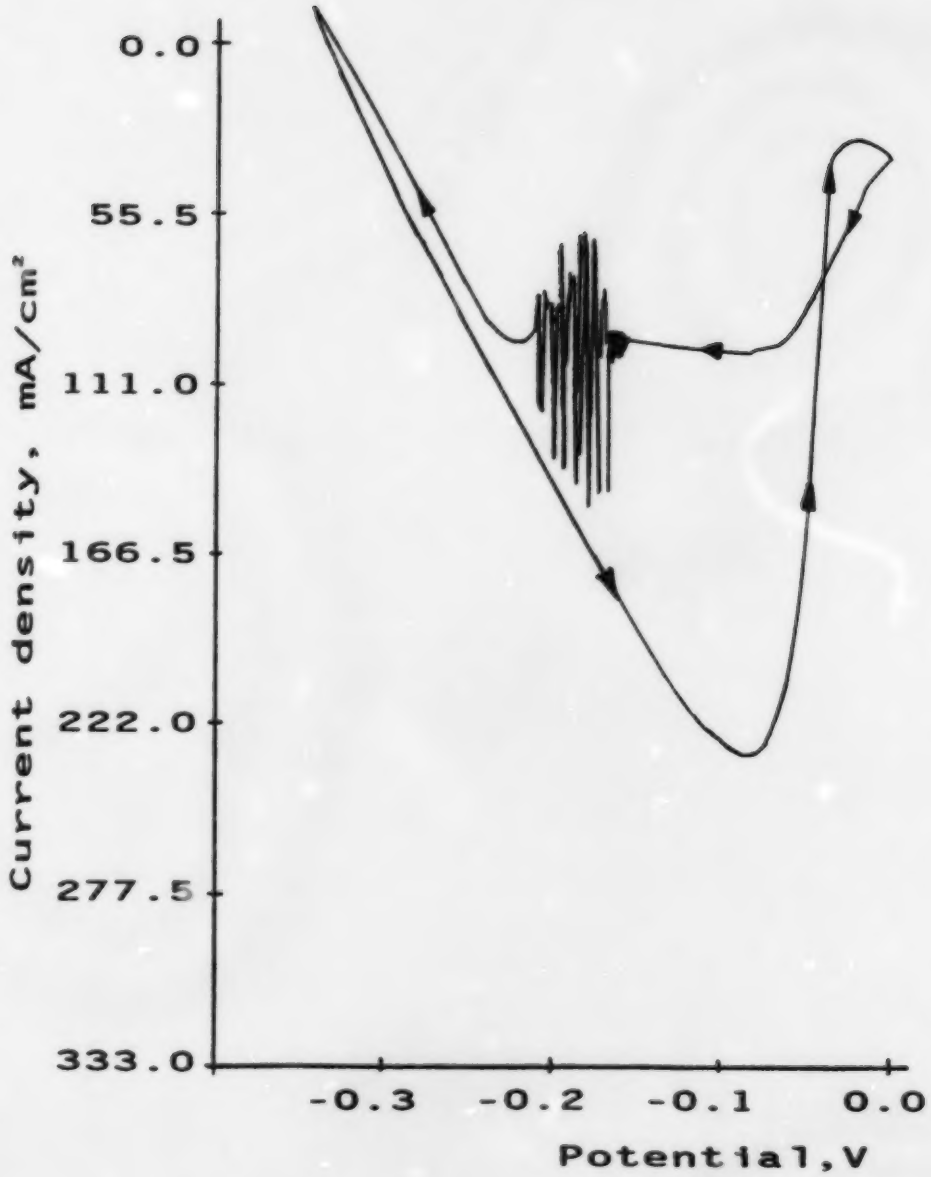

Figure 22. Cyclic voltammograms obtained for a Cu-1.0% Se anode showing the last (66th) cycle prior to SEM observation.

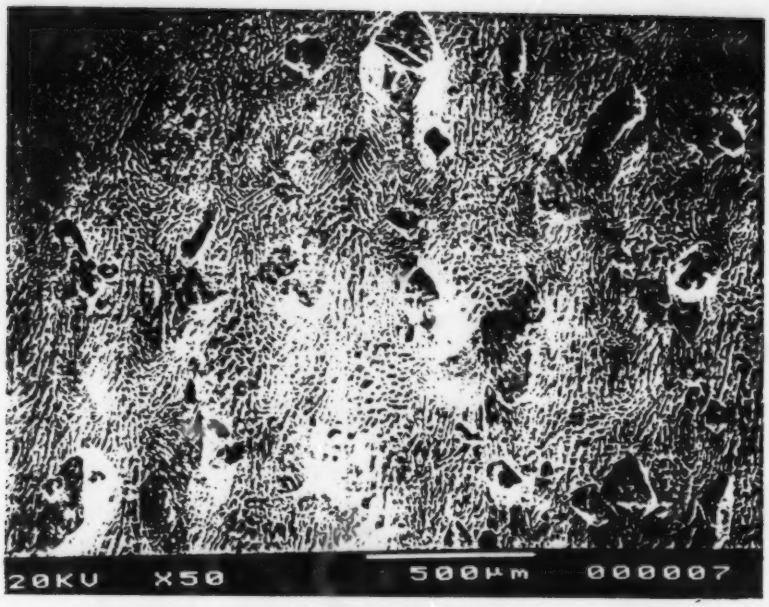

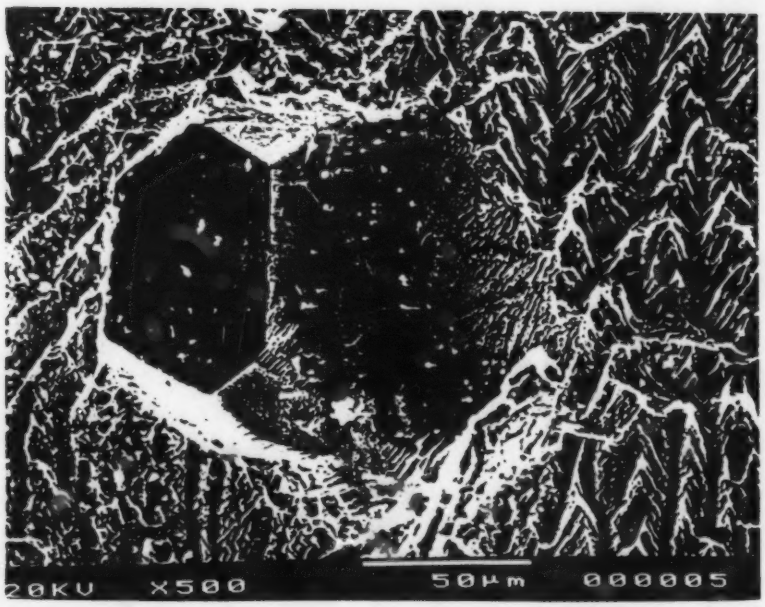

Figure 23. SE micrographs showing the morphology of the cleaned surface of a pure copper anode after 40 cycles.

Figure 24. SE micrographs showing the morphology of the cleaned surface of a Cu-0.1% Ag anode after 31 cycles.

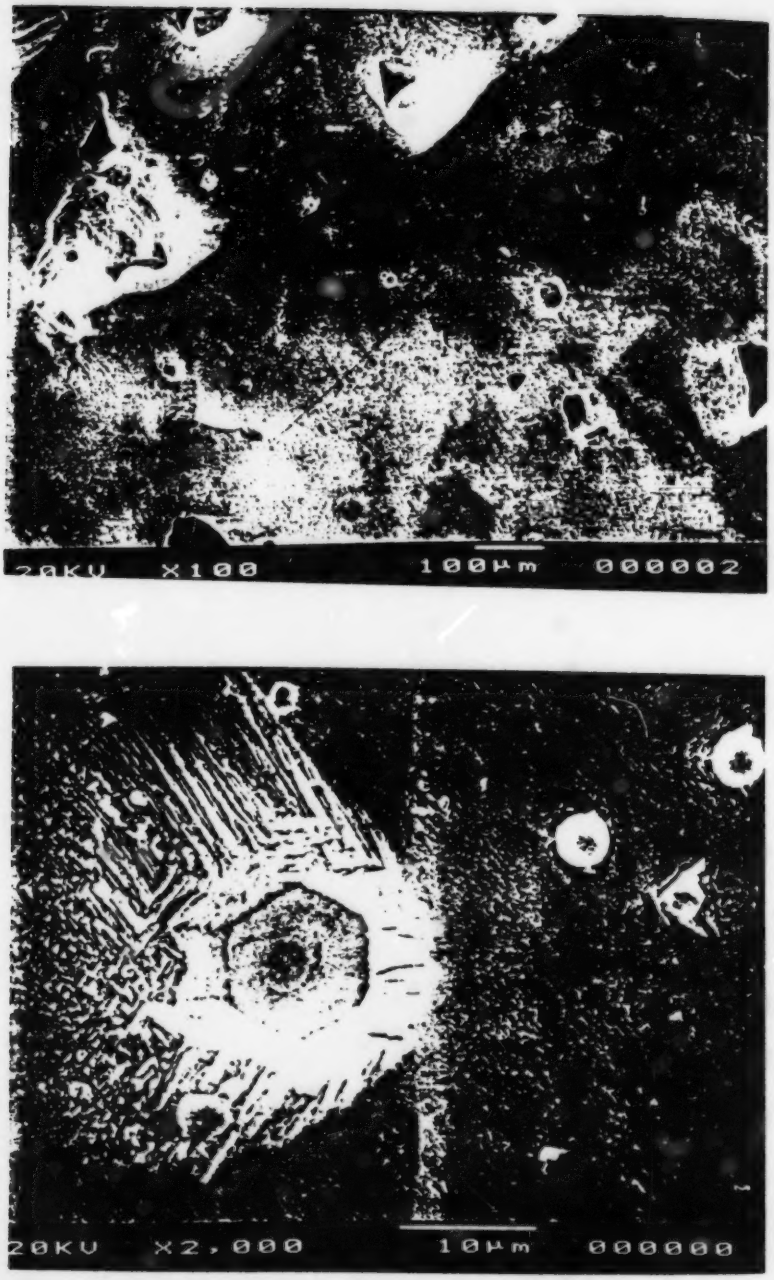

Figure 25. SE micrographs showing the morphology of the cleaned surface of a Cu-0.1% Se anode after 31 cycles.

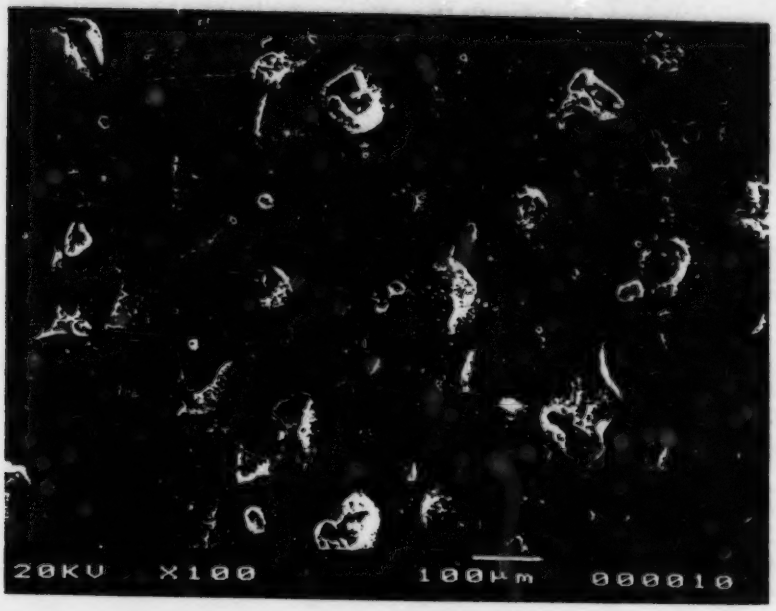

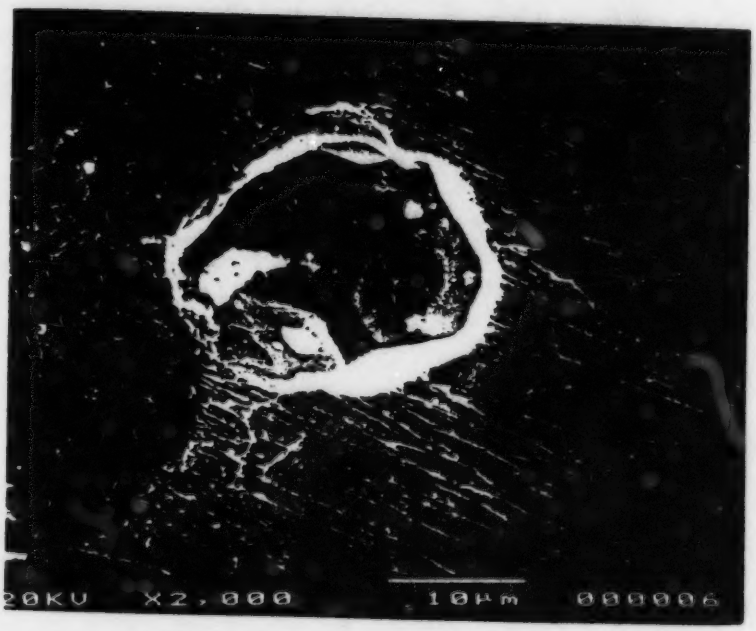

Figures 26. SE micrographs showing the morphology of the cleaned surface of a Cu-0.1% Se anode after 60 cycles.

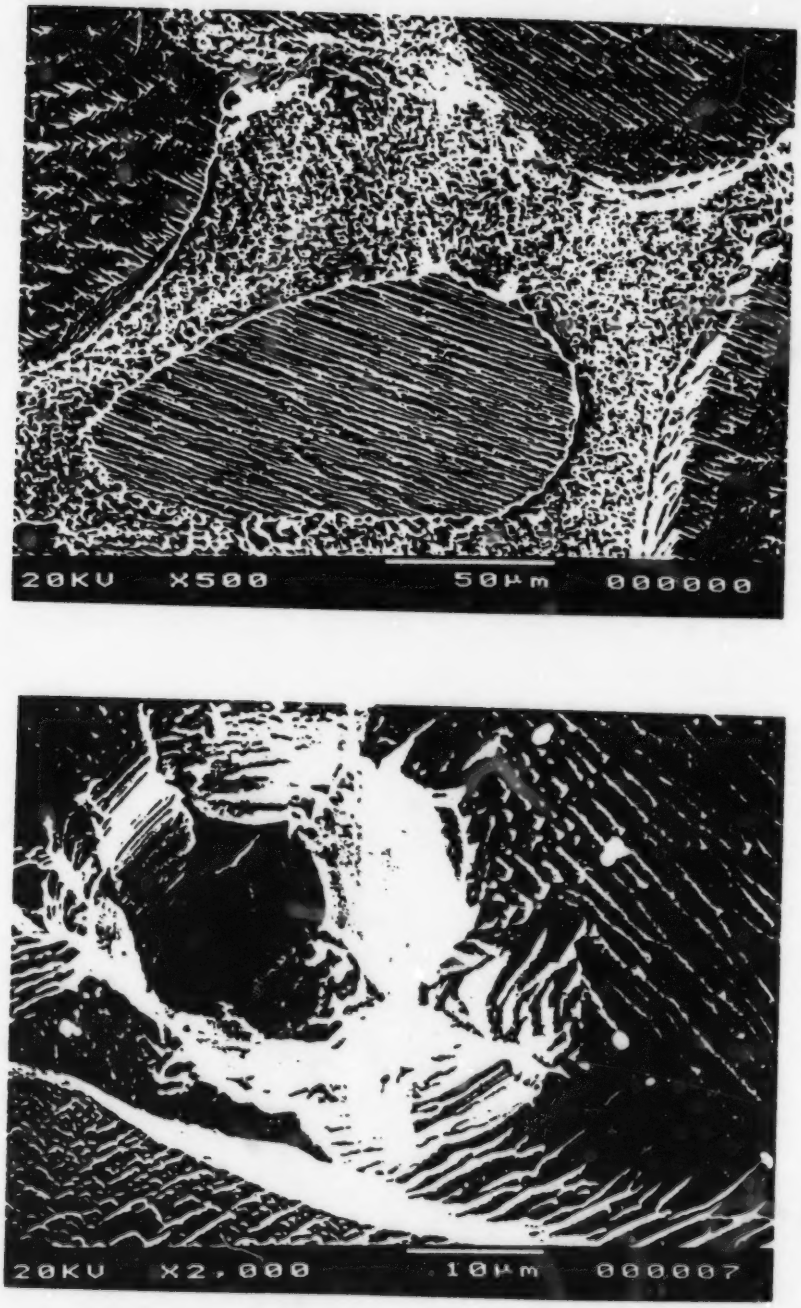

Figure 27. SE micrographs showing the morphology of the cleaned surface of a Cu-0.1% O anode after 31 cycles.

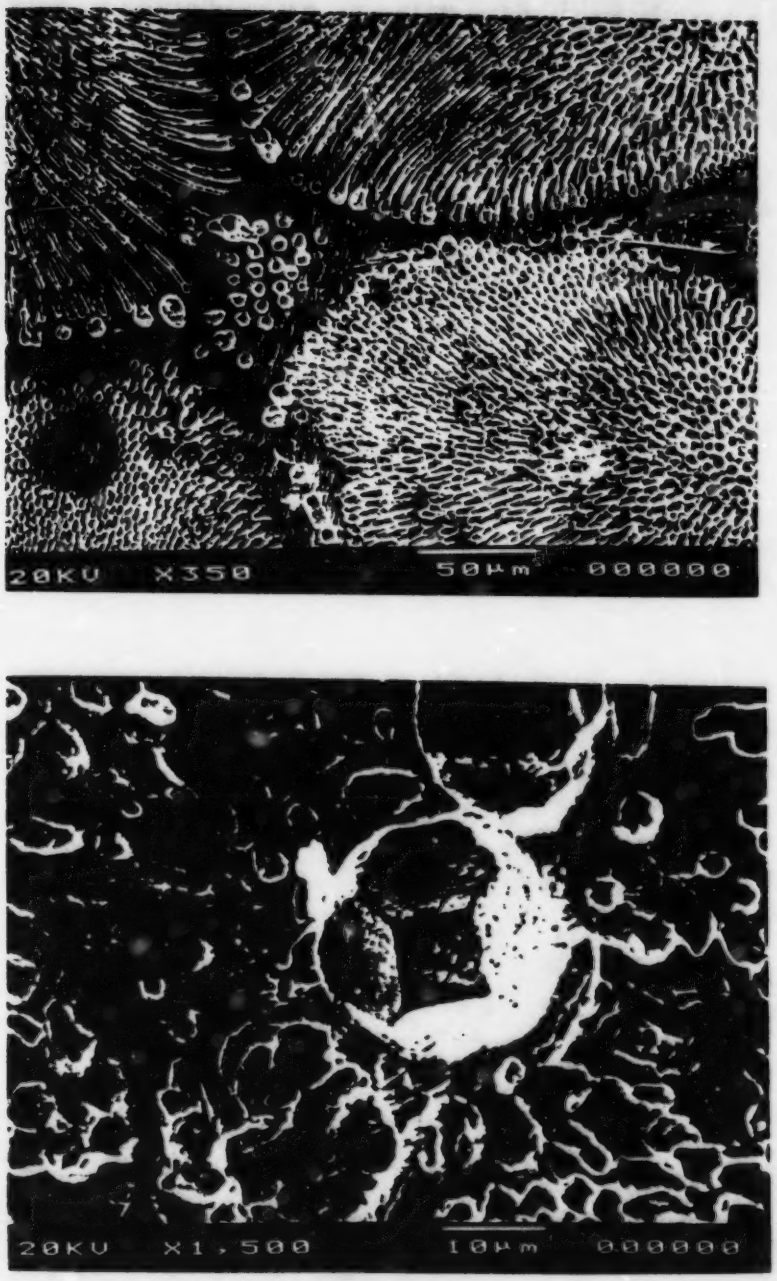

Figure 28. SE micrographs showing the morphology of the cleaned surface of a Cu-1.0% O anode after 36 cycles.

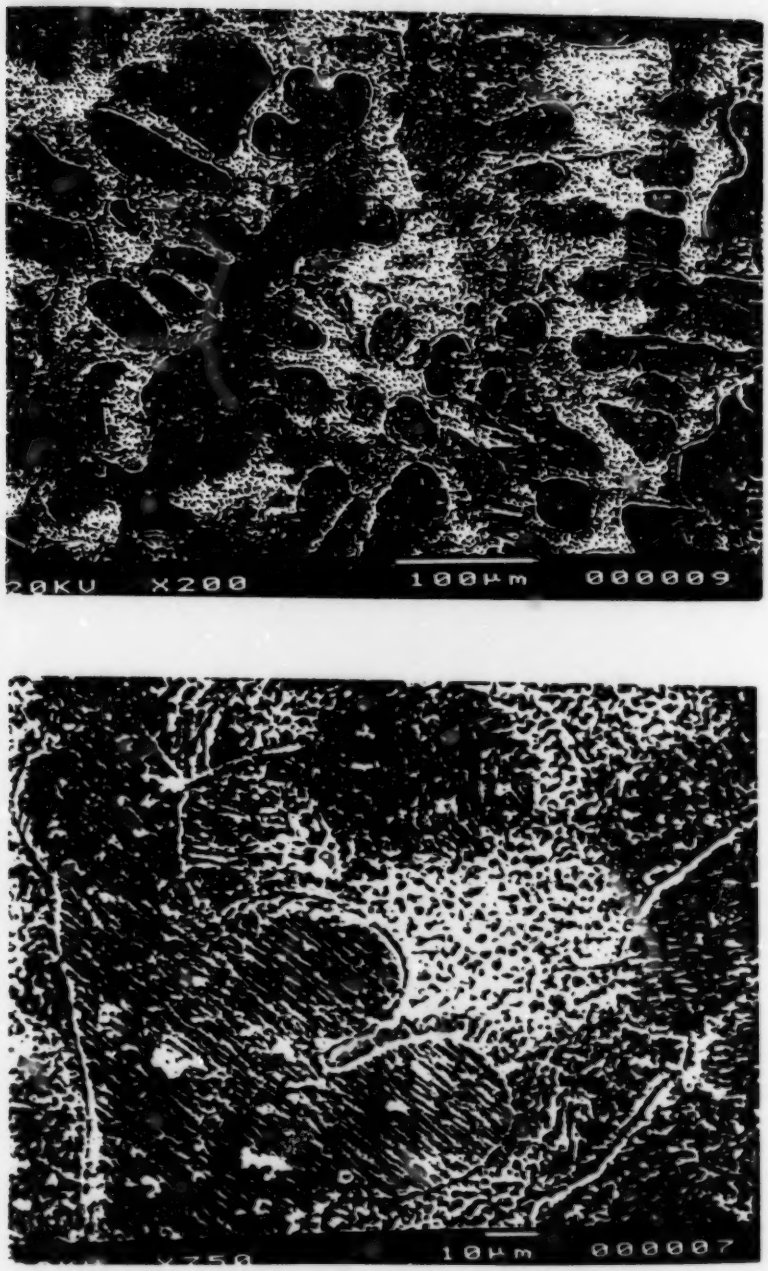

Figure 29. SE micrographs showing the morphology of the cleaned surface of a Cu-0.3% Ni +0.3% O anode after 27 cycles.

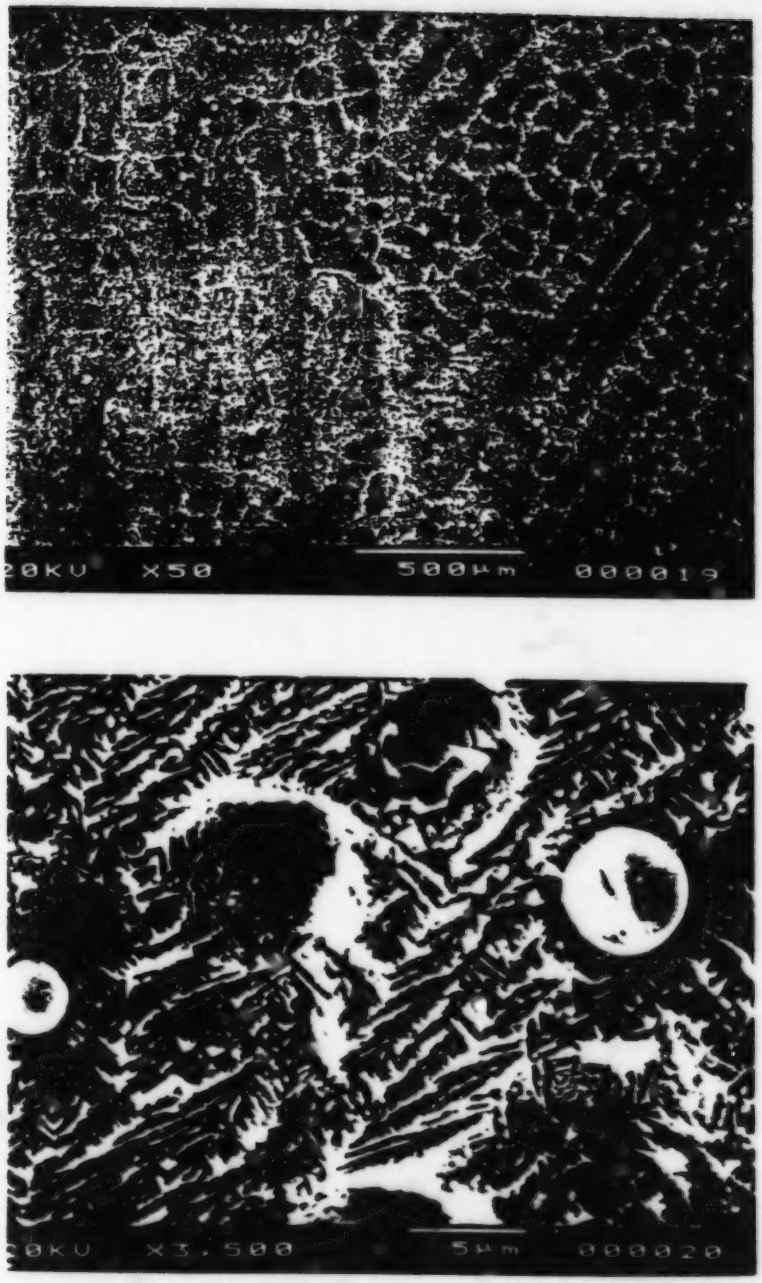

Figure 30. SE micrographs showing the morphology of the cleaned surface of a Cu-1.0% Se anode after 66 cycles. Rounded white particles are Cu_2Se spheroids.

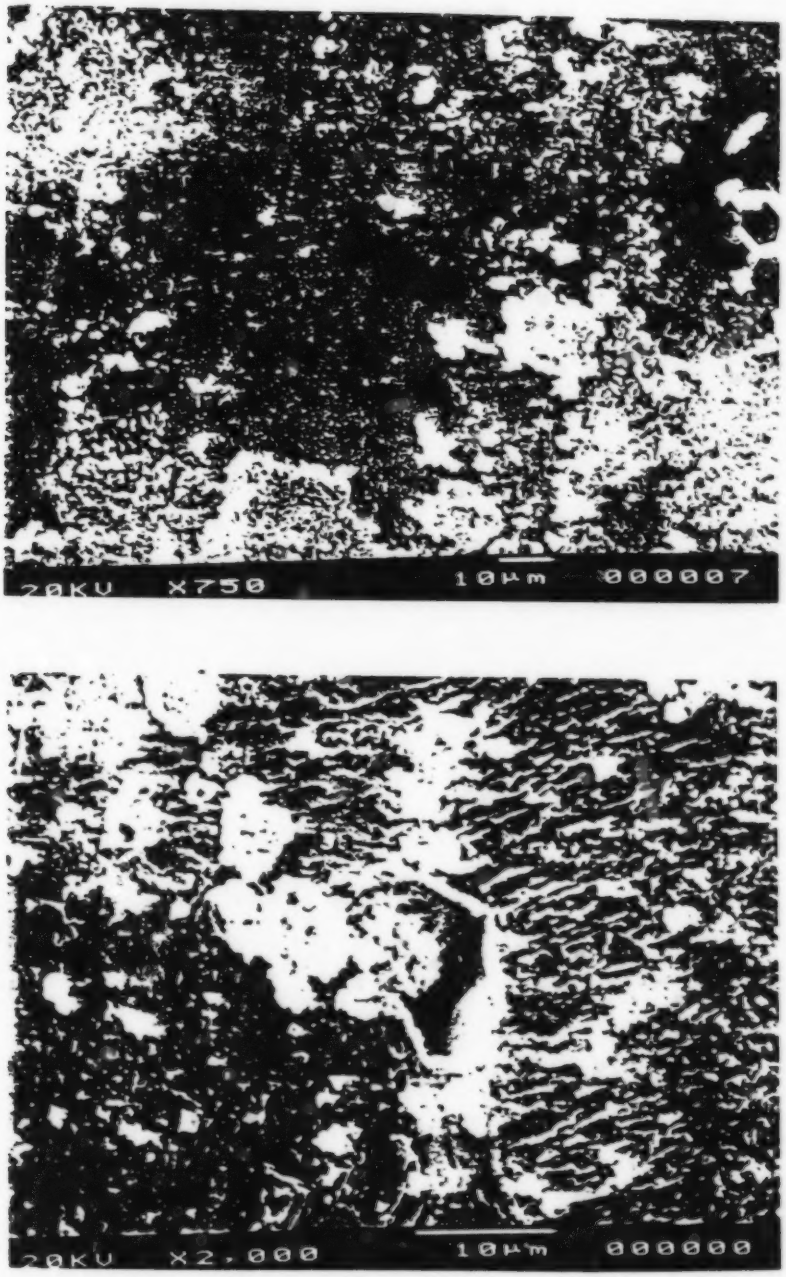

Figure 31. SE micrographs showing the morphology of the cleaned surface of a Cu-1.0% Ag anode after 30 cycles. White clusters are Ag powder.

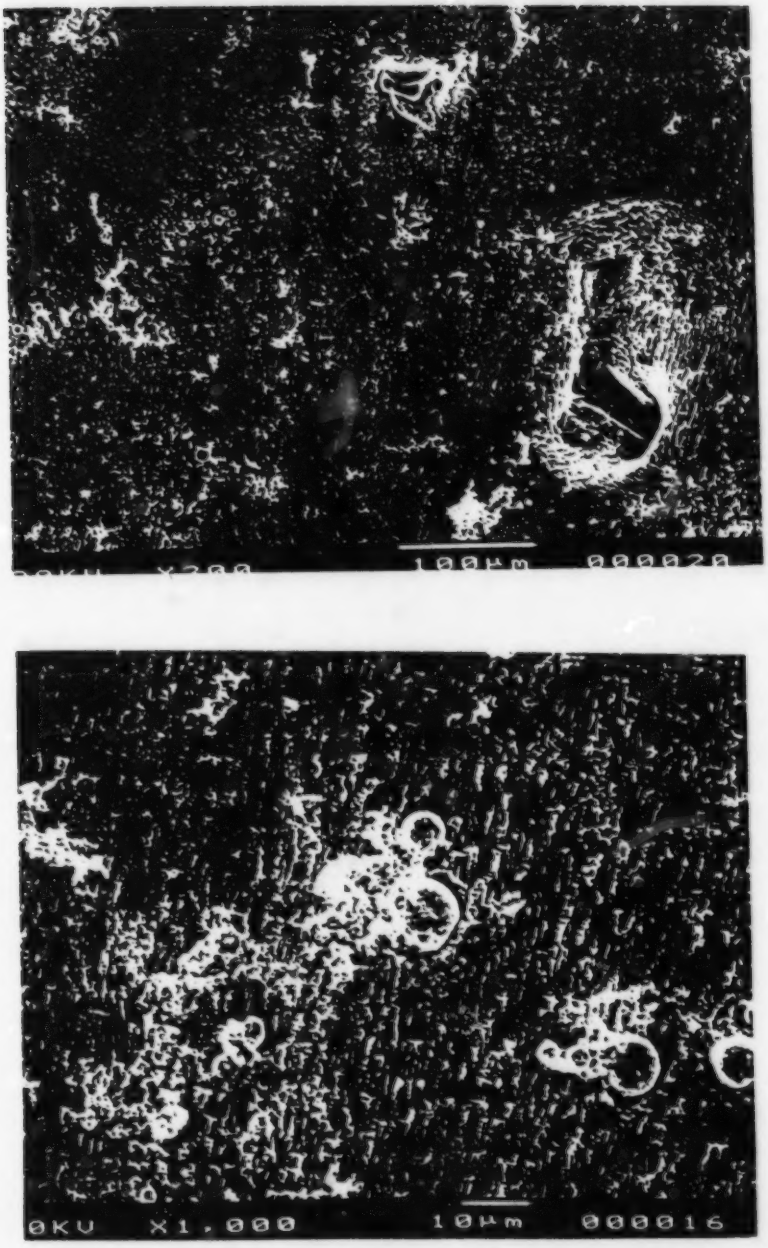

Figure 32. SE micrographs showing the morphology of the cleaned surface of a Cu-0.1% Ag + 0.1% Se anode after 47 cycles. Rounded particles are Cu_2Se spheroids.

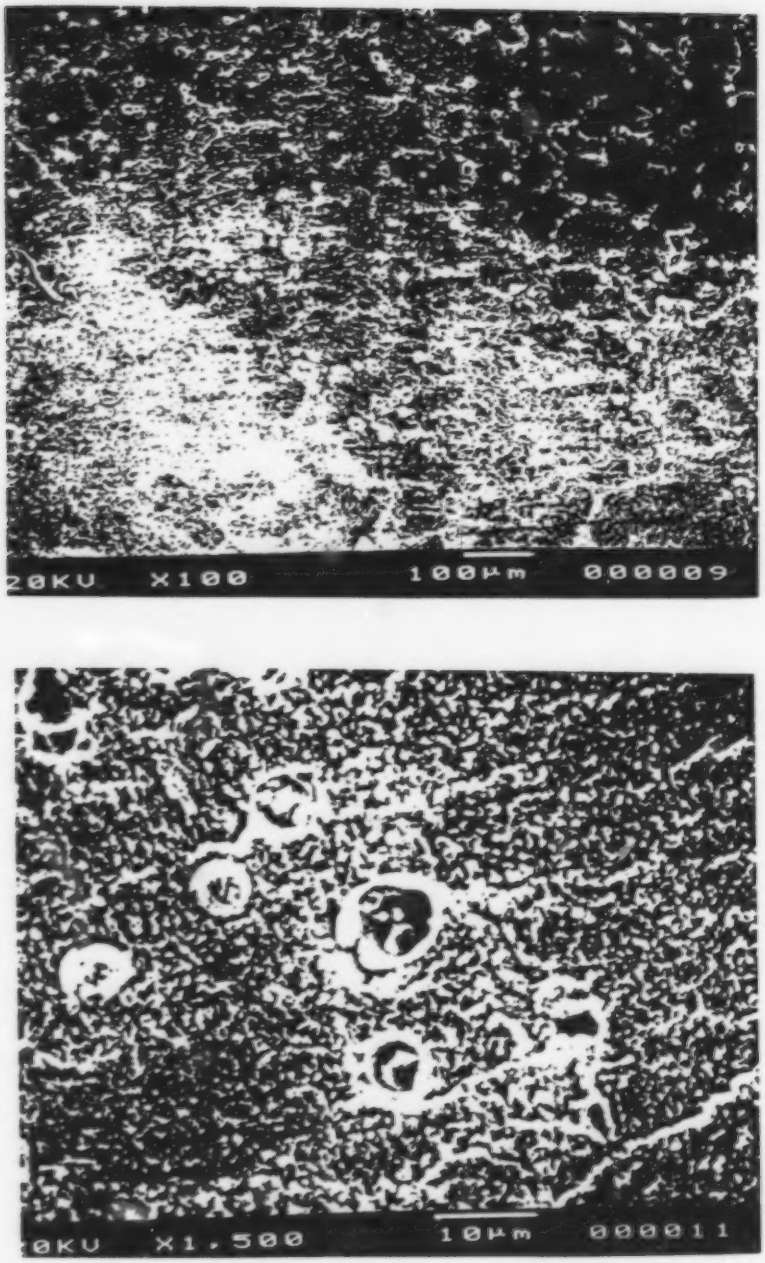

Figure 33. SE micrographs showing the morphology of the cleaned surface of a HBMS commercial anode after 32 cycles. Rounded particles are Cu_2Se spheroids.

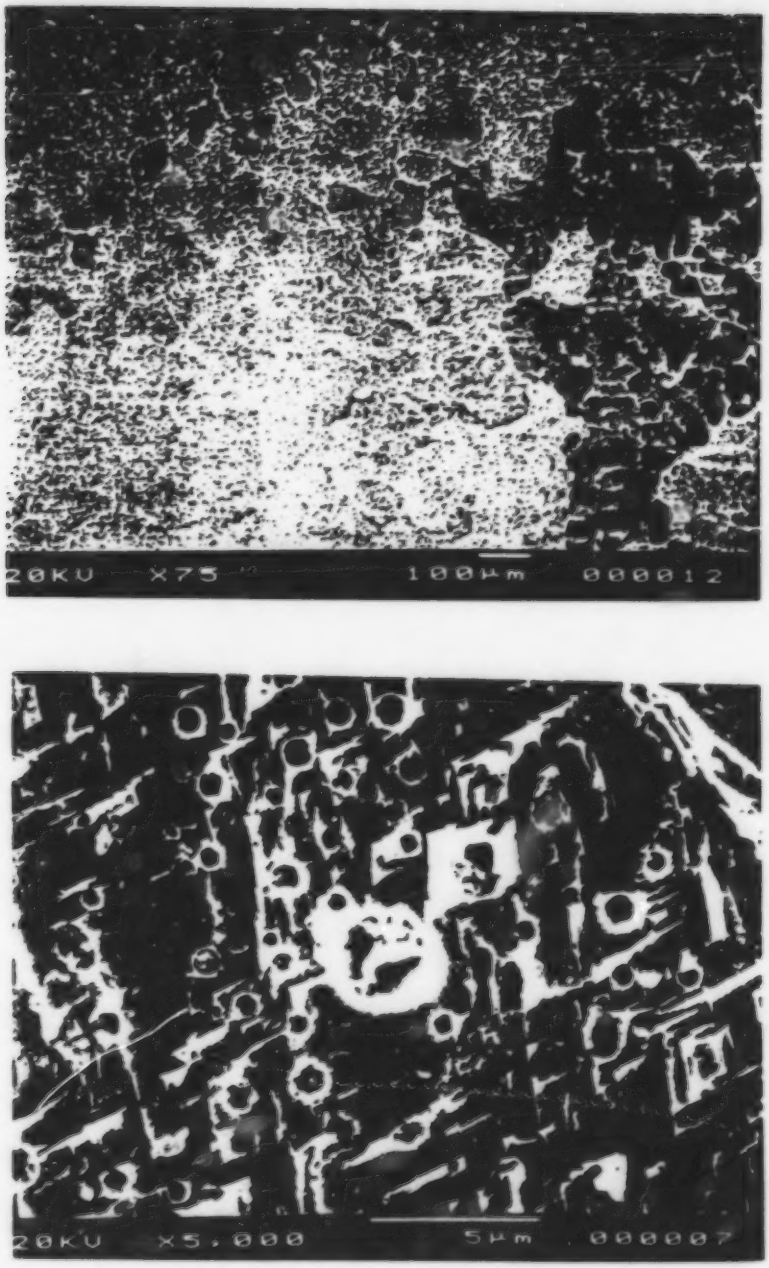

Figure 34. SE micrographs showing the morphology of the cleaned surface of a Kidd Creek commercial anode after 39 cycles. Holes are due to the release of Cu_2Se spheroids.

Figure 35. SE micrographs showing the morphology of the cleaned surface of a CCR commercial anode after 55 cycles. Rounded particles are Cu_2Se spheroids and the white clusters are Ag powder.